Technische Universität München
Zentrum Mathematik

Pattern Formation of Magnetic Nanoparticles on Surfaces

Andrea Elisabeth Kampfer

Vollständiger Abdruck der von der Fakultät für Mathematik der Technischen Universität München zur Erlangung des akademischen Grades eines

Doktors der Naturwissenschaften (Dr. rer. nat.)

genehmigten Dissertation.

Vorsitzender:		Univ.-Prof. Dr. Martin Brokate
Prüfer der Dissertation:	1.	Univ.-Prof. Dr. Dr. h.c. mult. Karl-Heinz Hoffmann
	2.	Univ.-Prof. Dr. Peter Rentrop
	3.	Priv.-Doz. Dr. Martin Kružík, Akademie der Wissenschaften Prag / Tschechien (schriftliche Beurteilung)

Die Dissertation wurde am 20.05.2010 bei der Technischen Universität München eingereicht und durch die Fakultät für Mathematik am 08.09.2010 angenommen.

Abstract

Magnetic nanoparticles on a surface form a pattern under the influence of an applied external magnetic field. This thesis encompasses the derivation of a new mathematical model for this pattern formation, its detailed analytical treatment and numerical simulation. The obtained model combines the concepts of micromagnetism with a particle distribution function first introduced by Cahn and Hilliard. The model takes into account the underlying physical forces and energies. The existence of a minimum of the free energy is proved by means of the direct method. For numerical simulation, the problem is considered as a constraint global minimization problem. The simulation results are in good agreement with the experimental data and therefore support the derived model.

Zusammenfassung

Unter dem Einfluss eines externen Magnetfeldes bilden magnetische Nanopartikel auf einer Oberfläche ein Muster. Diese Arbeit umfasst die Herleitung eines neuen mathematischen Modells, das diese Musterbildung beschreibt, dessen mathematische Analyse und numerische Simulation. Das verwendete Modell kombiniert mikromagnetische Beiträge mit einer Partikelverteilungsfunktion nach Cahn und Hilliard, wobei die relevanten physikalischen Effekte berücksichtigt werden. Durch die direkte Methode wird die Existenz eines Minimums der freien Energie gezeigt. Für die numerische Simulation wird das Problem als beschränktes globales Optimierungsproblem aufgefasst. Die Simulationsergebnisse stimmen gut mit experimentellen Ergebnissen überein und bestätigen somit das hergeleitete Modell.

Acknowledgement

First of all I would like to thank my advisor Prof. Dr. Dr. h.c. mult. Karl-Heinz Hoffmann for having confidence in me and for his support over the years. He encouraged this work and enabled my stay at caesar where I met various scientists that study nanoparticles.

I would like to thank the chemist Dr. Michael Hilgendorff who I met at caesar. He introduced me to the matter of nanoparticles and answered patiently my questions. He also made it possible for me to synthesize nanoparticles in the laboratory.

My special thanks go to Priv.-Doz. Dr. Martin Kružík for the various interesting and fruitful discussions during his stays in Munich and for his encouragement.

Financial support by the Deutsche Forschungsgemeinschaft through the graduate program "Angewandte Algorithmische Mathematik" at the Technische Universität München is gratefully acknowledged.

I thank my fellow members of the graduate program and my colleagues at the TU for their support. The discussions with you were motivating and brightened up my days.

I am indebted to Christian and Irmi for proofreading and helpful comments on my drafts.

Last but not least I would like to thank my boyfriend, my family and my friends for all their support, patience and encouragement during the ups and especially the downs while I was working on this thesis.

Contents

Table of symbols

This table of symbols cointains symbols that are not only used locally but throughout this document.

Greek letters

symbol	meaning
α	multiplier for Helmholtz free energy
μ_0	vacuum permeability, $\mu_0 = 4\pi \cdot 10^{-7}$ Vs/Am
χ_Ω	characteristic function on Ω
Γ	boundary of Ω
Γ_V	outer boundary of Ω_V
Ω	domain in $\mathbb{R}^2$ containing ferrofluid
Ω_V	domain in $\mathbb{R}^2$, necessary for calculation of potential V

Latin letters

symbol	meaning
u	particle distribution function
$\mathbf{m}$	scaled, oriented local magnetization vector
A	exchange stiffness constant

$C(\Omega)$	space of functions that are continuous on Ω
$\mathbf{H_d}$	Stray field
$\mathbf{H_{ext}}$	applied external magnetic field; unit: Ampere / meter
Hz	Hertz, unit of frequency; 1 Hz = 1 s^{-1}
$\mathbf{H_{sat}}$	saturation magnetization
$\mathbf{J}$	magentic polarization vector $\mathbf{J} = \mu_0 M_S \mathbf{m}$
J_S	saturation polarization, $J_S = \mu_0 M_S$
K_S	standard triangle, vertices (0,0), (1,0), (0,1)
M_S	saturation magnetization
T	Tesla, unit of a magnetic field; 1 T = 1 kg / (A s^2)
V	scalar potential of the stray field $\mathbf{H_d} = -\nabla V$
$W^{k,p}$	Sobolev space of functions $v \in L^p(\Omega)$ for which the partial derivatives $\partial^\alpha v$ are also in $L^k(\Omega)$ for all $\|\alpha\| \leq k$

Chapter 1

Introduction

The physicist and chemist Richard Feynman was the first to use the concepts of nanotechnology in his 1959 talk "There's plenty of room at the bottom" [1]. He imagined that one day the whole Encyclopaedia Britannica could be written on the head of a pin. Yet the term 'nanotechnology' was defined in 1974 by Tokyo Science University Professor Norio Taniguchi. It deals with the control of matter on the atomic and molecular scale, which is about 1-100 nm. Conveniently, a nanoparticle is defined as a particle with at least one dimension smaller than 100 nm.

Nanotechnology is a broad scientific topic that covers different sectors of science such as applied physics, material science, interface and colloid science, device physics, supramolecular chemistry and chemical, mechanical and electrical engineering. Last but not least, applied and numerical mathematics are indispensable tools to describe correctly and evaluate these processes.

In recent years, nanotechnology has attracted intense research interest as it provides solutions to many technological demands of the future. One prominent example is the need for high density data storage. This can be achieved by utilizing magnetic nanoparticles or nanostructured materials, which are the object of many research projects. The employment of nanoparticles is

also promising in medical science. Medical devices and drugs based on nanoparticles can detect and treat diseases more effectively and with fewer side-effects. In animal testing, it is already possible to direct nanoparticle loaded stem cells into damaged areas of the body where, for example, they enhance the repair of damaged tissue [2, 3].

Since only the size is restricted, nanoparticles are used in different areas and are made out of a variety of materials. Therefore, particles with diverse properties are gained. For example, iron (Fe), cobalt (Co) or compounds containing these are used for ferromagnetic nanoparticles. One industrially important application is the use of arrays of self-assembled monodisperse ferromagnetic nanoparticles for data storage, where each particle represents one bit of information. For this purpose, large arrays of regularly ordered particles are needed. The production of such an array is a very active field of research and was investigated by the nanoparticle technology group at the Center of Advanced European Studies and Research (caesar) in Bonn. This thesis is motivated by one of their experimental results. A drop of a ferrofluid, which is a liquid that contains ferromagnetic nanoparticles, is placed on a surface. Then the liquid dries out slowly while an external magnetic field is applied. The particles form a pattern that depends on the direction and strength of the applied field.

The aim of this thesis is the derivation of a model that describes the underlying physical process of this experiment, followed by its mathematical analysis and, finally, by its numerical simulation. In Chapter 2, a new mathematical model for the considered problem is derived, where the concepts of micromagnetism are combined with a particle distribution function first introduced by Cahn and Hilliard [4, 5]. Up to now, discrete models on a microscopic scale are used for the modeling of the considered problem. The discrete models are commonly solved by stochastic methods, e.g. Monte Carlo Simulation. In this thesis, a continuum model on a mesoscopic scale is developed, where the density of the particles is modeled instead of each

particle individually. For a better understanding, general information about the fabrication and processing of nanoparticles is given in Section 2.1, where also experimental results of different groups are shown. A general theory of magnetism is given in Section 2.2. Within this framework, a functional describing the free energy for the experiment considered is derived in Section 2.3 where the energy contributions due to different magnetic effects and due to particle interaction are explained separately.

This energy functional is discussed analytically in Chapter 3, where the existence of a minimum in an appropriate space is shown by means of the direct method of the calculus of variation. This method requires to prove the coercivity and the weak lower semicontinuity of the functional.

For the numerical simulation in Chapter 4, the model is at first reformulated and discretized in Sections 4.1 and 4.2. Since it is a constrained nonlinear global optimization problem, the terms and definitions of constrained global optimization are introduced and applied to the problem in Section 4.3, where adequate algorithms are also presented. Finally, the simulation results are displayed and discussed in Section 4.4. In particular, the different modeling parameters and their influence on the resulting particle distribution are studied. The good agreement between experimental results and simulations supports the derived model.

Chapter 2

Modeling

The aim of this chapter is the derivation of an equation that describes the free energy of following experiment: a drop of a fluid containing ferromagnetic nanoparticles is put to a surface. Under the influence of a magnetic field, the particles are free to move and rotate within the fluid. Taking a diluted suspension with a sufficiently low particle fraction, the particles assemble at the surface and form a pattern, which depends on the direction and intensity of the magnetic field.

First of all, nanoparticles are introduced, and production and handling of them are explained. Then experimental results are shown in Section 2.1.2, afterwards the basic principles of magnetism are illustrated in Section 2.2 and in Section 2.3 the energy equation is derived. This chapter concludes with stating the complete model.

2.1 Introduction to nanoparticle technology

A definition of nanoparticles is established first. Then synthesis, stabilization, application and assembling are discussed. The motivation for this thesis is elucidated in Section 2.1.2, where experimental results are shown. Nanoparticles are a complex topic thus in this thesis only a short introduction is given. An excellent review is given by [6].

2.1.1 Nanoparticles

There is no standard agreement on what to call **nanoparticle**, but typically it is defined as a particle with a diameter of 1-100 nm, consisting of a few up to some thousand atoms or molecules. If the particle is singlecrystalline, it might be called nanocrystal. A broad variety of substances and alloys is used to synthesize particles, for example cobalt (Co) and iron platinum alloys (FePt) are popular to build magnetic particles.
A solution in which nanoparticles are suspended is called a **colloidal solution**. In this thesis, dispersed ferromagnetic particles are considered, which are also called **ferrofluids**.

Synthesis

There are two general approaches to synthesize nanoparticles: either a big block of starting material is pulverized, which is called top-down approach, or particles are grown starting with precursors containing molecules and/or atoms. As the bottom-up approach provides suitable particles for the experiments, it is described below. There exist many recipes on the bottom-up synthesis of nanoparticles, but more or less particles are prepared according to following procedure:
Precursors are mixed with a solvent and with a stabilizer if required, then heated to reflux or kept at room temperature for a certain time, which could be supported by bubbling with N_2,

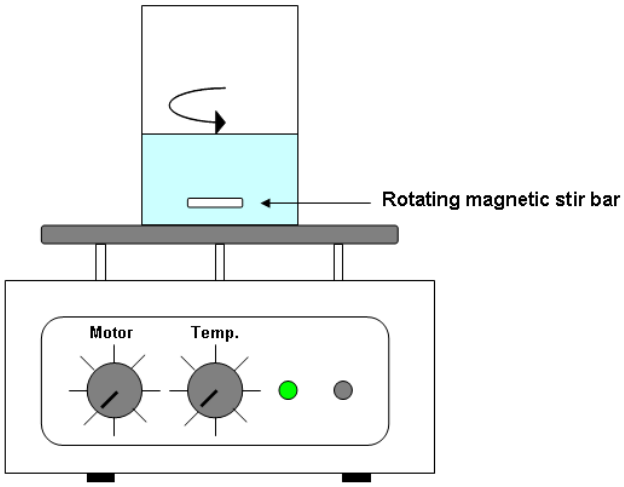

Figure 2.1: Sketch of a magnetic stirrer with a heating facility. The magnetic stir bar inside the vessel is moved by a rotating magnet under the hot-plate.

Ar or another substance. For stirring, a magnetic stirrer is used, which is shown in figure 2.1. This device is often combined with a heating facility. A vessel containing the mixture and a magnetic stir bar is put on a hot-plate, under which a magnet rotates and moves the bar thereby. After the mixing and heating process, the particles have about the suitable size for application. So they are transferred to another solvent in order to stop the growth process.
At that point, particles of different sizes coexist in the solution. For application, monodisperse particles are necessary, as then also the sum of attractive and repulsive forces between colloidal particles is narrowly distributed and therefore the ferrofluid is homogeneous. Depending on the desired particle size, oversized and undersized ones have to be extracted, whereas advantage is taken of different properties of different sized particles. Bigger magnetic particles and aggregates, which may also appear, possess a stronger magnetic moment. They stick to the magnetic stir bar and are therefore easily removed by removing the bar. Then the larger of the remaining particles are extracted by using a magnet with different properties. They are transferred to

a different solvent. Adding e.g. ethanol destabilizes the smaller particles, they aggregate and precipitate. The size of the precipitating particles is controlled by the concentration of the added substance. Finally particles of a narrow size distribution remain. If the size distribution is 5 % or lower, the particles qualify as monodisperse.

The size selection process is labor-intensive, an unknown amount of particles is extracted and therefore the particle concentration afterwards is unknown. Since the concentration is important for application, it has to be determined in a labor-intensive process: Using a magnet, the particles are extracted from the solution and washed repeatedly in order to remove excess substances from the production process. Then the particles are dried in an evaporator such that their weight can be determined. After the determination of the weight, the concentration of the main substance, e.g. Co, within a particle is still unknown. By assuming a certain thickness of the oxide shell and of the surfactant, which have different chemical and physical properties, this concentration is determined and therefore the particle properties are known.

Once a solution of monodisperse particles is obtained, and the concentration is determined, the colloidal solution needs to be stabilized.

Stabilization

In order to prevent particle agglomeration, repulsive forces are needed to overcome the omnipresent attractive Van der Waals forces and - in the case of magnetic particles - the magnetic dipole-dipole interactions. This is achieved either through electrostatic or through steric repulsion. Electrostatic repulsion requires charged particles in an aqueous media, where positively charged particles occur in acidic solutions and negatively charged in alkaline media. To provide for steric repulsion, the particles are coated with a stabilizing layer. The shell may also protect the particles against oxidation and erosion through acids and bases.

The binding between particles and stabilizers occurs either through physisorption, where sta-

bilizers can be exchanged and therefore the particles can be transferred from non-aqueous to aqueous systems. Or the binding results from chemisorption, where no further ligand exchange is possible, but which is required e.g. for non-noble particles of larger size.

Depending on particle composition and application, the appropriate stabilizing technique has to be chosen. Especially for medical application, one has to pay attention to a biocompatible layer. Commonly used is coating by tensides, polymers, noble metals, silicate and carbon. Through controlled oxidation metallic particles are coated by a non reactive oxide surface, which leads to stable particle solutions.

Application

In medicine, biocompatible nanoparticles promise for new therapies in cancer treatment and are used as carrier for a precise drug delivery. Moreover, new materials, integrated cooling systems for refrigerators and new inks for inkjet printers could be constructed by using nanoparticles. Because of the small dimension, they have a higher surface to volume ratio and hence they are highly reactive and efficient catalysts, and magnetic ones are easy to re-extract.

Highly symmetric monolayers (i.e. two dimensional systems) of ferrofluids are of much interest scientifically and of great importance technologically, as they promise to be a building block for a new generation of magnetic storage devices. For practical application, ordered structures of several square millimeters are needed.

Different methods are used to create particle monolayers on a surface, the most important are described in the following.

Assembling

Drying a drop of colloidal solution on a flat substrate is the commonly used method of assembling nanoparticles. The size of sheets of symmetric ordered particles depends on the surface,

the stabilizer and the particle matter. If no external field is applied, it is called **self assembling** (SA). By adding an external field, the symmetry and the size of the sheets are enhanced. An electric field acts on charged particles, while for ferromagnetic or superparamagnetic particles a magnetic field is required. This most promising method is called **magnetophoretic deposition method** (MDT). The strength and the direction of the magnetic field influence the size and the shape of the particle sheets significantly, as shown in Section 2.1.2, figure 2.2. Compared to SA, the interparticles distance is decreased, while the distance between clusters of ordered particles is increased, cf. [7].

The ordering process takes some time to be completed, during which the solvent is needed, as it allows the particles to move and to align according to the laws of physics.

Throughout this thesis, it is assumed that the particle movement requires a significant smaller time than the drying process. Hence the ordering is quasi stationary compared to the drying. Due to this reason the ordering process is considered time independent and thus a stationary model is established.

2.1.2 Experiments

An observation made by the Nanoparticle Technology group at caesar motivated this thesis: if a drop of colloidal solution is applied on the surface of a substrate and dried under the influence of an external magnetic field, the pattern formed by the particles is determined by the direction and strength of the applied field, see figure 2.2, which is taken from [8]: in the lower part it shows transmission electron microscopy (TEM) images of ordered domains of monodisperse Co particles with a diameter of 12 nm, where the standard deviation is about 5 %. In the upper part the respective experimental assemblies are displayed. The particles are stabilized with toluene or o-xylene, which are aromatic hydrocarbons. They are deposited on carbon-coated copper grids using MDT. The results on the left of figure 2.2 are gained by applying magetic fields of

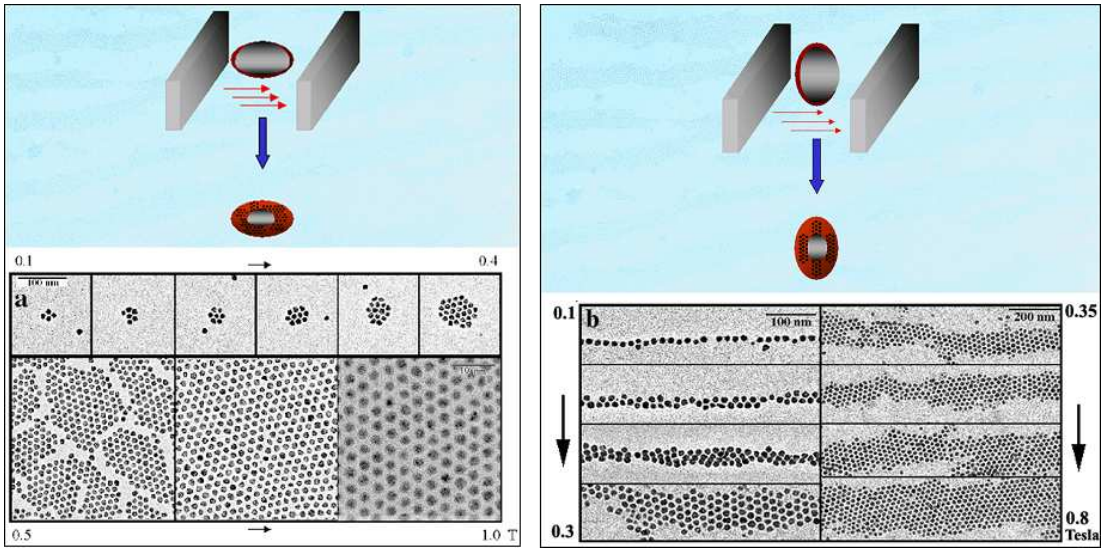

Figure 2.2: Transmission electron microscopy (TEM) image, taken from [8], of ordered domains of 12 nm diameter Co particles.

0.1 to 1 T parallel to the substrate. The size of the particle domains obviously increases with increasing applied magnetic field. The results for a magnetic field of 0.1 to 0.8 T perpendicular to the substrates are displayed on the right side of figure 2.2. As here the substrate is also perpendicular to the ground, the formation of chains might result from gravitational forces. These pictures show that the width of the chains increases with an increased applied magnetic field, regardless whether the field is parallel or perpendicular to the substrate. Since according to [8] by MDT two-dimensional arrays of near perfect symmetry up to 1 μm^2 in size are received on various substrates, the influence of the substrate is not considered in the model.

Also Hayes [10] observes that ferrofluids form chains or needles under the influence of a magnetic field. These needles are big enough to be detected by light scattering, which was used to produce pictures. For figure 2.3 an altering magnetic field was used, but he states that a static field would lead to the same structures. The influence of the magnetic field is evident: (A) is received without an applied field, (B) with an applied oscillating magnetic field of $5 \cdot 10^{-4}$

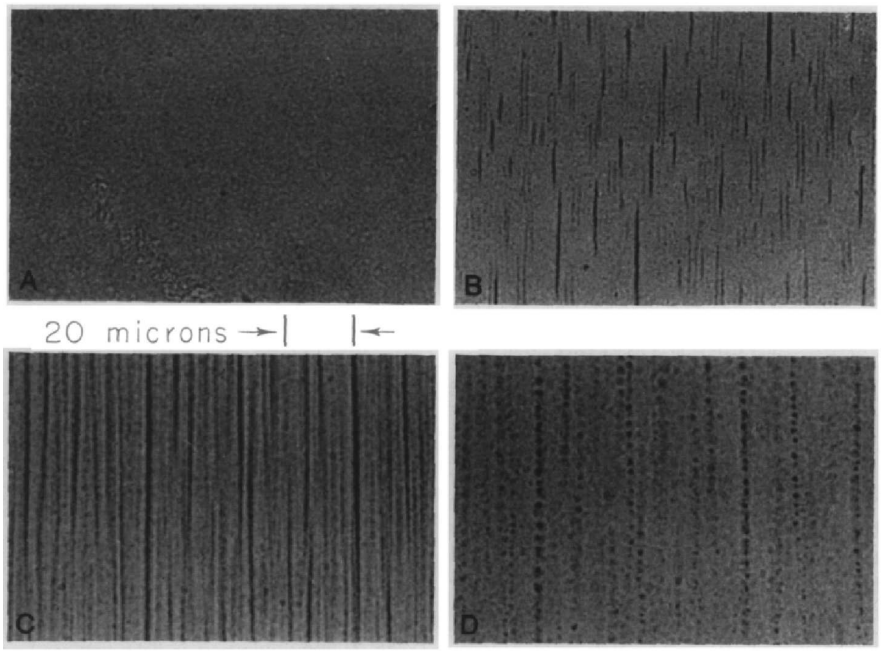

Figure 2.3: Micrographs of a ferrofluid taken from [10]

T at 60 Hz, (C) with an applied field of $2.1 \cdot 10^{-3}$ T at 60 Hz and (D) with a field suddenly decreased to zero. The long axes of the needles are parallel to the applied magnetic field.

There exist various simulation studies about the chainlike clusters observed in [10]. The commonly used method is Monte Carlo Simulation (MCS), where the energy of a starting configuration is minimized by a stochastic process, in which one particle is identified by one bit of information. For example, Satoh et al. [11] successfully simulates the chainlike structure, where the results show dependence on the strength of the applied magnetic field $\mathbf{H_{ext}}$, compare figure 2.4. Not only the structures align according to $\mathbf{H_{ext}}$, but also the magnetic moments of the particles, which are marked by a dash.

In this thesis a continuum model on a mesoscopic scale is developed instead of the discrete, stochastic model on a microscopic scale. As by MCS the optimal position is individually calculated for every particle, this method is limited by computational power to the simulation of

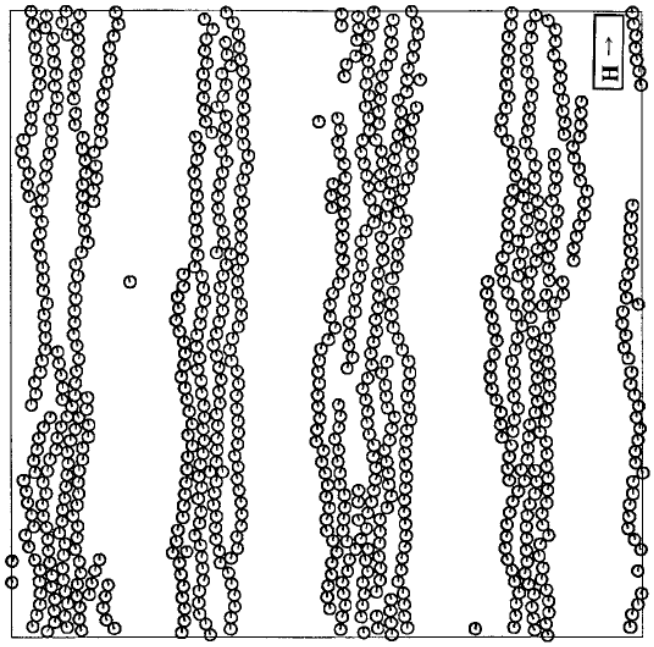

Figure 2.4: Chains by Monte Carlo simulation, taken from [11].

systems consisting of only several hundreds of particles. By introducing a distribution function $u(\mathbf{x})$ not each particle is individually modelled, but the density of particles. This enables simulations of bigger systems.

2.1.3 Basic modeling assumption

As stated in Section 2.1, a stationary continuous model is considered. The stationarity leads to the assumption of a constant temperature.

The free energy of a ferrofluid that is influenced by an external magnetic field is searched. This energy is to be minimized due to the laws of physics. The contributions to the free energy are here divided into two parts:

- energy contributions due to magnetic phenomena and
- energy contributions due to particle distribution and interaction,

where the latter may also cover magnetic phenomena.

The particles are assumed to form a monolayer on a surface, which is equivalent to a thin film. This suggests that the magnetic energy is described by the theory of thin magnetic films, which is called micromagnetism. The physical background of micromagnetism is outlined in Section 2.2, afterwards the magnetic energy contributions are derived in Section 2.3.1.

In order to calculate the energy contributions due to particle distribution and interaction, one should keep in mind that a ferrofluid is isotropic and incompressible. These properties are prerequisites for the application of the Cahn-Hilliard model of free energy of the phase distribution of a two component system. This contributions are elucidated in Section 2.3.2.

2.2 Concepts of micromagnetism

The previous section deals with nanoparticles in general. Obviously, the behavior of magnetic particles in an applied magnetic field is influenced by their magnetic properties. To understand these effects, this section studies magnetism. Basic notations of magnetism, ferromagnetism and micromagnetism are introduced and some basic magnetic principles are illustrated. For further details which are beyond the scope of this short introduction see [12, 13]. [14] provides a deep insight into magnetic microstructure.

The **magnetization** of a device is defined as the **magnetic moment** per unit volume. In the following, both terms will be used. The concept of **micromagnetism**, which is the continuum theory of magnetic moments, was first formulated over 70 years ago by Landau and Lifshitz, see [15].

2.2.1 Magnetism

The magnitude and the direction of a magnetic system is measured by the magnetic moment. A ferromagnet has a spontaneous magnetic moment, i.e. a magnetic moment even without an applied magnetic field. The existence of a spontaneous moment suggests that magnetic moments are arranged in a regular manner. In a ferromagnet they are essentially parallel on a microscopic scale. This alignment is quantum-mechanically explained by exchange forces [13]. Thermal agitation, which is opposed to the spontaneous magnetization, tends to destroy the spin order, such that the spontaneous magnetization decreases if the temperature increases. It vanishes completely above the **critical** or **Curie temperature** (T_C = 1041 K or 768° C for iron), when ordering is only obtained by applying an external magnetic field $\mathbf{H_{ext}}$. So above T_C the ferromagnet acts like a paramagnet, which classifies a material, within which an applied external field is fortified. Single domain nanoparticles (see Section 2.2.3 for a definition) exhibit similar behavior even below T_C and above a blocking temperature: the magnetic moments within each particle are aligned to form one "super"-moment, but because of thermal agitation the supermoments change direction and therefore the system acts paramagnetic. This phenomenon is called **superparamagnetism**.

Saturation magnetization and polarization

The maximal induced magnetic moment that can be obtained in an applied external magnetic field $\mathbf{H_{ext}}$ is called **saturation magnetization** (M_S). The minimal field that is needed to generate M_S is the saturation field $\mathbf{H_{sat}}$. Increasing $\mathbf{H_{ext}}$ even further beyond $\mathbf{H_{sat}}$ does not change the magnetization. The saturation magnetization is an intrinsic material property, which is temperature-dependent and can be measured experimentally. Instead of the saturation magnetization sometimes the **saturation polarization** $J_S = \mu_0 M_S$ is specified, where

$\mu_0 = 4\pi \cdot 10^{-7}$ Vs/Am is the vacuum permeability. In literature, these notations are used inconsistently and sometimes synonymously but in this thesis the definition above holds.

Values of the saturation magnetization and polarization are well known for bulk material. For example, [12] specifies values for ferromagnetic crystals, where the saturation polarization ranges from 1 T to 3 T, depending on the temperature and the matter: J_S increases with decreasing temperature.

For the saturation magnetization of nanoparticles, the stabilizing layer has to be considered. Be D the diameter of the particle and t the constant thickness of the layer, which is assumed to be non-magnetic. Then the saturation magnetization $M_S(D)$ of the particle is derived from the bulk saturation magnetization M_{S0}, cf. [16]

$$M_S(D)/M_{S0} = 1 - 6t/D \quad .$$

Obviously, this relation also holds for the saturation polarization $J_S(D)$ of a particle and the bulk saturation polarization J_{S0}. However, the thickness t is not known but a fitting parameter to experimental results. Depending on the bulk material, it is about 0.5 - 0.7, see [16].

Assuming a particle size of 12 nm and $t = 0.5$ leads to $J_S(D) = 0.75 \cdot J_{S0}$, thus the saturation polarization of ferromagnetic particles is about 0.75 to 2.25 T.

2.2.2 Magnetic domains

The spontaneous magnetic moment of a ferromagnetic specimen may be much smaller than its saturation magnetization. This effect occurs because the specimen are composed of small domains, the so-called **Weiss domains**. Weiss domains are small areas in the crystal structure of a ferromagnetic material with parallel - according to the local structure of the material - oriented magnetic momenta. Within each domain the magnetization is locally saturated, but the magnetic moments among different domains may not be parallel. The different domains are

separated by domain walls. The size of these oriented domains is in the range of 10^{-3} to 10^{-5} mm, including a volume of about 10^6 to 10^9 atoms. By applying a magnetic field, the volume of the favorably oriented domains grows at the expense of the unfavorably oriented ones. Under the influence of a strong applied field, the magnetic orientation of all domains rotates towards the direction of the field.

2.2.3 Magnetic particles

As the size of a magnetic specimen or a magnetic particle decreases towards some critical particle diameter, the formation of domain walls becomes energetically unfavorable and the particles consist of only one Weiss domain. Therefore they are called **single domain**, compare [17].

Since the dimension of nanoparticles is approximately 10^{-5} mm, which is roughly the size of a domain, the assumption of single domain nanoparticles is justified. Throughout this thesis $|\mathbf{H_{ext}}| \geq |\mathbf{H_{sat}}|$ is assumed, such that the magnetization of the particles is saturated. Only a finite external field, i.e. $|\mathbf{H_{ext}}| < \infty$, makes sense physically.

In a dynamic magnetic system, hysteresis has to be considered, but this thesis concentrates on a stationary model. The stationarity is also the reason why the temperature is assumed to be constant within the system, so the saturation magnetization is constant, too.

2.2.4 Magnetic field

When speaking of *magnetic field* one has to distinguish between the **B**-field and the **H**-field, which is also called auxiliary magnetic field. While the magnetic flux density, magnetic field or magnetic induction **B** is measured in Tesla (T), the unit of the magnetic field intensity, magnetic field strength or magnetizing field **H** is Ampere per meter. In free space, they are

connected by the vacuum permeability μ_0:

$$\mathbf{B} = \mu_0 \cdot \mathbf{H} \tag{2.1}$$

Equation (2.1) holds for free space. If a magnetic body is located in the magnetic field, the magnetic field is changed. Be $\Omega \subset \mathbb{R}^2$ the domain occupied by a magnetic body, whose magnetic polarization is $\mathbf{J}$. It generates a magnetic field itself, the so-called **stray field**, which influences the general magnetic field. Let χ_Ω be the characteristic function on Ω, which means $\chi_\Omega(\mathbf{x}) = 1$ for $\mathbf{x} \in \Omega$ and $\chi_\Omega(\mathbf{x}) = 0$ for $\mathbf{x} \in \mathbb{R}^2 \setminus \Omega$, and be $\mathbf{H_d}$ the generated stray field, then

$$\mathbf{B} = \mu_0 \mathbf{H_d} + \chi_\Omega \mathbf{J} \quad . \tag{2.2}$$

Gauss's law for magnetism, which is one of Maxwell's equations, states that magnetic monopoles do not exist. In other words, the magnetic field $\mathbf{B}$ is solenoidal, which is expressed by div $\mathbf{B} = 0$. Employing equation (2.2) yields

$$\text{div } (\mu_0 \mathbf{H_d} + \chi_\Omega \mathbf{J}) = 0 \quad . \tag{2.3}$$

In the absence of electric current and field - as in the considered model - Ampère's law states $\nabla \times \mathbf{H_d} = 0$. Thus in this case, the magnetic field is irrotational. As $\nabla \times (\nabla V) = 0$ holds for any scalar valued potential function V, $\mathbf{H_d}$ is substituted by $-\nabla V$. It is to be noted that V is defined on the whole space $\mathbb{R}^2$. Outside Ω in the absence of magnetic matter, where $\mathbf{m} = 0$, equation (2.3) yields $\Delta V = 0$.

2.2.5 Recapitulation

After discussing the physical background of magnetism and micromagnetism, the mathematical context of the variables is specified.

This thesis considers the pattern formed by monolayered particles on a surface, therefore the model is restricted from the in reality three dimensions to two dimensions. Be $\Omega \subset \mathbb{R}^2$ the

domain occupied by the particle solution and be $\mathbf{J}(\mathbf{x})$ the local magnetic polarization vector, which indicates the direction and the intensity of the local magnetization at position $\mathbf{x}$. Inside Ω, it is the product of the scaled and oriented local magnetization $\mathbf{m}(\mathbf{x})$, where $|\mathbf{m}(\mathbf{x})| = 1$, and of the saturation polarization J_S, so

$$\mathbf{J}(\mathbf{x}) = J_S \cdot \mathbf{m}(\mathbf{x}) = \mu_0 M_S \cdot \mathbf{m}(\mathbf{x}) \quad . \tag{2.4}$$

Due to the absence of magnetic matter, $\mathbf{J}(\mathbf{x})$ vanishes outside of Ω:

$$\mathbf{J}(\mathbf{x}) \equiv 0 \qquad \forall\, \mathbf{x} \in \mathbb{R}^2 \setminus \Omega \quad . \tag{2.5}$$

In real world, the magnetic moment is free to rotate in three dimensions, but in the model it is only considered in a two-dimensional domain. Taking the projection on the two-dimensional domain into account, the restriction $|\mathbf{m}(\mathbf{x})| \leq 1$ is sufficient.
The local magnetization is considered as a function $\mathbf{m} : \Omega \to \mathbb{R}^2$. Whenever needed, this function is expanded to $\mathbf{m} : \mathbb{R}^2 \to \mathbb{R}^2$, where $\mathbf{m}(\mathbf{x}) \equiv 0$ holds for all $\mathbf{x} \in \mathbb{R}^2 \setminus \Omega$.

2.3 Energy equation

As stated in Section 2.1.3, the energy of the studied problem consists of the magnetic energy, which is explained in Section 2.3.1, and the energy due to particle interaction, which is explained in Section 2.3.2.

2.3.1 Magnetic energy

According to the classical model for stationary micromagnetics due to Weiss, Landau, and Lifshitz [14, 15], four different energy contributions add up to the magnetic energy of thin layers:

- the **anisotropy energy**,
- the **Zeeman energy**,
- the **exchange energy** and
- the **stray field energy**.

The energy functional E is minimized over an admissible set of magnetizations $\mathbf{m} : \Omega \rightarrow \mathbb{R}^2$.

Anisotropy energy

In a ferromagnetic crystal, certain crystallographic axes exist, the so-called easy axes, along which the spontaneous magnetization is preferably aligned. The easy axes are connected to the structure of the crystal. The anisotropy energy measures the deviation of the magnetic moment from the easy axes.

$$E_{an}(\mathbf{m}) = \int_{\Omega} \varepsilon_{an}^{loc}(\mathbf{m}) \, d\mathbf{x} \ ,$$

where the local anisotropy density $\varepsilon_{an}^{loc}(\mathbf{m})$ for cubic crystals is given by

$$\varepsilon_{an}^{loc}(\mathbf{m}) = K_1(m_x^2 m_y^2 + m_x^2 m_z^2 + m_y^2 m_z^2) + K_2(m_x^2 m_y^2 m_z^2) \ \ ,$$

where K_1 and K_2 are material constants and the three-dimensional magnetization vector is given by $\mathbf{m} = (m_x, m_y, m_z)^T$.

In the case of a uniaxial anisotropy, where the x-axis is energetically favored, this can be simplified to

$$\varepsilon_{an}^{loc}(\mathbf{m}) = K_u(1 - m_x^2) \qquad (K_u > 0). \tag{2.6}$$

Since in this thesis the nanoparticles are considered free to rotate, they will align such that the easy axis points in direction of the magnetic field. Therefore the anisotropy energy will be minimized to be equally zero and will not be considered in the calculation.

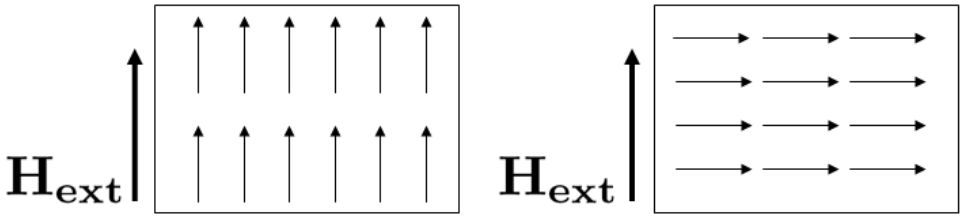

Figure 2.5: The **Zeeman energy** is lower in the case on the left side, where the magnetic moments are aligned according to the external field $\mathbf{H_{ext}}$.

Zeeman energy

The applied external field $\mathbf{H_{ext}}$ provokes the Zeeman energy

$$E_Z(\mathbf{m}) = -J_S \int_\Omega \mathbf{H_{ext}} \cdot \mathbf{m} \; d\mathbf{x} \quad . \tag{2.7}$$

For a uniform external field, this energy is determined only by the average magnetization and it is independent of the sample shape and the particular domain structure, compare [14]. Figure 2.5 illustrates the Zeeman energy for two different magnetization directions: It is lower in the case on the left, where the magnetic moments are aligned according to the external field. On the right, the magnetic moments are perpendicular to the external field.

$|\mathbf{H_{ext}}| \geq |\mathbf{H_{sat}}|$ is assumed, which effects saturation magnetization in the particles.

Exchange energy

In a ferromagnet, a homogeneous direction of magnetization is energetically favored. Deviations thereof invoke an energy penalty, which can be described by

$$E_x(\mathbf{m}) = A \int_\Omega |\boldsymbol{\nabla} \mathbf{m}|^2 \; d\mathbf{x} \,, \tag{2.8}$$

see [14]. The operator $\boldsymbol{\nabla}$ generates the gradient of a vector, e.g. applied to $\mathbf{a} = (a_1, a_2)^T$ we get in detail $|\boldsymbol{\nabla} \mathbf{a}|^2 = |\nabla a_1|^2 + |\nabla a_2|^2$.

The so-called exchange stiffness constant A (dimension J/m or erg/cm) is a weakly temperature dependent material constant. At constant temperature a constant value of A is taken. For ferromagnetica it is within the range of $10^{-12} - 2 \cdot 10^{-11}$ J/m, cf. [14].

Equation (2.8) is derived by a Taylor expansion of the isotropic Heisenberg interaction between neighboring spins, compare [14]. Since the energy is independent of the direction of the change relative to the magnetization direction, it is called isotropic.

Stray field energy

As derived in Section 2.2.4, the stray field $\mathbf{H_d}$ is defined by equation (2.3), which equals

$$\text{div } \mathbf{H_d} = -\text{div } (\chi_\Omega \mathbf{J}/\mu_0) \quad .$$

Taking the scalar potential V, where $\nabla V = -\mathbf{H_d}$, and recalling $\mathbf{J} = J_S \cdot \mathbf{m} = \mu_0 M_S \cdot \mathbf{m}$ leads to

$$\begin{aligned} \Delta V &= M_S \,\text{div } (\chi_\Omega \mathbf{m}) \qquad (2.9) \\ \Delta V &= \text{div } \left(\chi_\Omega \frac{\mathbf{J}}{\mu_0} \right) \;\Rightarrow\; \frac{\mu_0}{J_S} \Delta V = \text{div } (\chi_\Omega \mathbf{m}) \\ \mathbf{H_d} &= -\nabla V = -\frac{J_S}{\mu_0} \nabla \left(\Delta^{-1} \text{div} \, (\chi_\Omega \mathbf{m}) \right) \;\Rightarrow\; V = \frac{J_S}{\mu_0} \Delta^{-1} (\text{div} \, (\chi_\Omega \mathbf{m})) \quad , \end{aligned}$$

where this equation holds in a distributional sense.

Now equation (2.9) is tested by V and integrated over the whole space $\mathbb{R}^2$. Since the magnetic field intensity decreases with increasing distance to the magentic device, it approaches zero at infinity. Thus V is constant at infinity and is w.l.o.g. assumed to be zero. Therefore the boundary condition for $\mathbf{x} \to \infty$ is given by $V(\mathbf{x}) \to 0$. Integration by parts and obeying the

factor χ_Ω yields:

$$\begin{aligned} \Delta V &= \operatorname{div}\left(\chi_\Omega \frac{\mathbf{J}}{\mu_0}\right) \\ \int\limits_{\mathbb{R}^2} \Delta V \cdot V \, d\mathbf{x} &= \int\limits_{\mathbb{R}^2} \operatorname{div}\left(\chi_\Omega \frac{\mathbf{J}}{\mu_0}\right) V \, d\mathbf{x} \\ \int\limits_{\mathbb{R}^2} \nabla V \, \nabla V \, d\mathbf{x} &= \int\limits_{\mathbb{R}^2} \chi_\Omega \frac{\mathbf{J}}{\mu_0} \nabla V \, d\mathbf{x} = \int\limits_{\Omega} \frac{\mathbf{J}}{\mu_0} \nabla V \, d\mathbf{x} \end{aligned}$$

Therefore energy of a body in its own field is given by

$$\begin{aligned} E_d(\mathbf{m}) = \frac{\mu_0}{2} \int\limits_{\mathbb{R}^2} {\mathbf{H_d}}^2 \, d\mathbf{x} = \frac{\mu_0}{2} \int\limits_{\mathbb{R}^2} |\nabla V|^2 \, d\mathbf{x} &= -\frac{1}{2} \int\limits_{\Omega} \mathbf{H_d} \cdot \mathbf{J} \, d\mathbf{x} \\ &= \frac{1}{2} \int\limits_{\Omega} \nabla V \cdot \mathbf{m} \, J_S \, d\mathbf{x} \\ &= \frac{J_S^2}{2\mu_0} \int\limits_{\Omega} \nabla(\Delta^{-1} \operatorname{div} \mathbf{m}) \cdot \mathbf{m} \, d\mathbf{x} \ . \end{aligned} \tag{2.10}$$

Compendium

Summing up the different magnetic energy contributions given by (2.6), (2.7), (2.8) and (2.10) leads to the classical model for the energy E^c_{mag} of stationary micromagnetics

$$\begin{aligned} E^c_{mag}(\mathbf{m}) &= E_{an}(\mathbf{m}) + E_Z(\mathbf{m}) + E_x(\mathbf{m}) + E_d(\mathbf{m}) \\ &= \int\limits_{\Omega} \varepsilon^{loc}_{an}(\mathbf{m}) \, d\mathbf{x} - J_S \int\limits_{\Omega} \mathbf{H_{ext}} \cdot \mathbf{m} \, d\mathbf{x} \\ &\quad + A \int\limits_{\Omega} |\boldsymbol{\nabla} \mathbf{m}|^2 \, d\mathbf{x} + \frac{J_S^2}{2\mu_0} \int\limits_{\Omega} \nabla(\Delta^{-1} \operatorname{div} \mathbf{m}) \cdot \mathbf{m} \, d\mathbf{x} \\ &= \int\limits_{\Omega} \left(\varepsilon^{loc}_{an}(\mathbf{m}) - J_S \, \mathbf{H_{ext}} \cdot \mathbf{m} + A \, |\boldsymbol{\nabla} \mathbf{m}|^2 - \frac{1}{2} J_S \, \mathbf{H_d} \cdot \mathbf{m} \right) d\mathbf{x} \ . \end{aligned}$$

Since in this thesis $E_{an}(\mathbf{m}) = 0$ is assumed, the energy is given by

$$\begin{aligned} E^c_{mag}(\mathbf{m}) &= \int\limits_{\Omega} \left(-J_S \, \mathbf{H_{ext}} \cdot \mathbf{m} + A \, |\boldsymbol{\nabla} \mathbf{m}|^2 - \frac{1}{2} J_S \, \mathbf{H_d} \cdot \mathbf{m} \right) d\mathbf{x} \\ &= \int\limits_{\Omega} \varepsilon^{loc}_{mag}(\mathbf{m}) \, d\mathbf{x} \ . \end{aligned}$$

The classical model holds for a continuous thin film of magnetic material but the nanoparticles are irregularly distributed on the surface and thus there is no continuous film. There are even particle-free spots, compare figure 2.2. Since the local magnetic energy contribution depends certainly on the thickness of the magnetic material, this thesis uses a new approach, which expands the classical model accordingly. Therefore the local magnetic energy density $\varepsilon_{mag}^{loc}(\mathbf{m})$ is combined with the particle density u such that the newly developed magnetic energy contribution is

$$E_{mag}(\mathbf{m}, u) \quad = \quad \int_{\Omega} \varepsilon_{mag}^{loc}(\mathbf{m}) \cdot u \; d\mathbf{x} \quad .$$

2.3.2 Energy due to particle interaction

For the total energy, besides the magnetic energy contribution also energy due to the particle interaction and distribution has to be taken in account. This contribution is derived in the following section.

Particle fraction

The fraction of particles in the domain $\Omega \subset \mathbb{R}^2$ will be denoted by the continuous distribution function $u : \Omega \to [0, 1]$. The value of u is bounded by 1, which equals 100% particles. $u(\mathbf{x}) = 0$ indicates a particle-free spot $\mathbf{x}$. The distribution function might be expanded to a function defined on the whole space such that $u : \mathbb{R}^2 \to \mathbb{R}$, where for $\mathbf{x} \in \mathbb{R}^2 \setminus \Omega$ the equality $u(\mathbf{x}) \equiv 0$ holds. Since the amount or mass of particles is conserved,

$$\int_{\Omega} u \, d\mathbf{x} = C_{\Omega} = c_{\Omega} \cdot |\Omega|$$

holds. Here c_{Ω} denotes the particle fraction in the domain Ω with surface area $|\Omega|$.

Cahn-Hilliard equation

This thesis considers a particle-liquid mixture. It is a two component system, which is assumed to be isotropic and incompressible. A general approach to calculate the free energy of a two component system at a fixed temperature is proposed by Cahn and Hilliard, cf. [4, 5].

The free energy equals the integral of the local free energy over the considered domain. The local free energy f is a function of the particle distribution u and its derivatives, which are considered as independent variables: $f(u, \nabla u, \nabla^2 u, \nabla^3 u, ...)$.

The function f is expanded in a Taylor series about $f_0(u) = f(u, 0, 0, ..)$ up to second rank terms. The subscript zero indicates that the value is considered in a solution of uniform composition, so f_0 is the free energy of a solution of uniform composition u. This implies particularly that f_0 is independent of $\mathbf{x}$. As the system is isotropic, the equation has to be invariant under the symmetry operations of reflection and rotation. Therefore only the even-ranked terms are considered and the expansion is reduced to

$$f(u, \nabla u, \nabla^2 u, ...) \approx f_0(u) + \left[\frac{\partial f}{\partial \nabla^2 u}\right]_0 \nabla^2 u + \frac{1}{2}\left[\frac{\partial^2 f}{\partial |\nabla u|^2}\right]_0 |\nabla u|^2 \quad , \tag{2.11}$$

where the subscript zero indicates that the terms in brackets are evaluated at $(u, 0, 0, ...)$.

Cahn and Hilliard [4] introduce the notation

$$\left[\frac{\partial^2 f}{\partial |\nabla u|^2}\right]_0 := \left[\frac{\partial^2 f}{\partial \left(\partial u \,/\, \partial x_i\right)^2}\right]_0 \quad .$$

As the energy has to be invariant under the above-mentioned symmetry operations, the term is equal for all i.

Integrating by parts and setting

$$\frac{\varepsilon^2}{2} = -\left[\frac{d}{du}\frac{\partial f}{\partial \nabla^2 u}\right]_0 + \frac{1}{2}\left[\frac{\partial^2 f}{\partial |\nabla u|^2}\right]_0$$

change (2.11) to

$$f(u, \nabla u, \nabla^2 u, ...) \approx f_0(u) + \frac{\varepsilon^2}{2}|\nabla u|^2 \quad .$$

For a more detailed derivation see [4].

The Helmholtz free energy $W(u) = f_0(u)$ is specified in the following paragraph.

Integration over these two terms leads to the free energy according to Cahn and Hilliard

$$E_{part}(u) = \int_{\Omega} W(u) + \frac{\varepsilon^2}{2}|\nabla u|^2 \, d\mathbf{x} \, . \tag{2.12}$$

Since the ordering of particles in a a sheet is regular and highly symmetric, this thesis considers the Taylor expansion up to fourth rank terms. The equation still has to be invariant under the symmetry operations of reflection and rotation, therefore only the even-ranked terms are additionally considered, which are following:

$$\begin{aligned} & \frac{1}{24}\left[\frac{\partial^4 f}{\partial|\nabla u|^4}\right]_0 |\nabla u|^4 + \frac{1}{6}\left[\frac{\partial^3 f}{\partial|\nabla u|^2\partial\nabla^2 u}\right]_0 |\nabla u|^2\nabla^2 u \\ + \quad & \frac{1}{2}\left[\frac{\partial^2 f}{\partial\nabla^2 u\partial\nabla^2 u}\right]_0 |\nabla^2 u|^2 + \frac{1}{2}\left[\frac{\partial^2 f}{\partial\nabla^3 u\partial\nabla u}\right]_0 \nabla^3 u\nabla u + \left[\frac{\partial f}{\partial\nabla^4 u}\right]_0 \nabla^4 u \end{aligned}$$

By partial integration, this sum of five terms is reduced to a sum of three terms. For calculation, any or a sum of these terms might be used, compare [19]. For this thesis, only the first term containing $|\nabla u|^4$ is chosen, as it possesses good analytical properties. In order to differentiate between the two coefficients ε, the assigned subscript corresponds to the exponent and (2.12) is expanded to

$$E_{part}(u) = \int_{\Omega} W(u) + \frac{\varepsilon_2^2}{2}|\nabla u|^2 + \frac{\varepsilon_4^2}{4}|\nabla u|^4 \, d\mathbf{x} \tag{2.13}$$

Generally spoken, $\frac{\varepsilon_2^2}{2}$ and $\frac{\varepsilon_4^2}{4}$ are 'interaction' lengths, which are small compared to characteristic dimensions on the laboratory scale. Different values for ε_2 and ε_4 are tested numerically in Section 4.4.3.

Helmholtz free Energy W(u)

The free energy density W is a smooth double well potential such that (see figure 2.6)

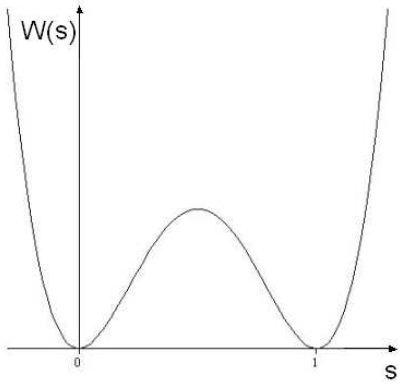

Figure 2.6: A symmetric double well potential $W(s)$ that satisfies constraints (2.14)

$$W(s) \geq 0 \qquad \forall s \in [0,1] \text{ and} \tag{2.14}$$

$$W(s) = 0 \qquad \Longleftrightarrow \quad s \in \{0,1\} \quad .$$

A general approach is

$$W(u) = a\left[(1-u)\ln(1-u) + u\ln u\right] + b(1-u)u$$

with dependent constants a and $b(a)$. Typically this is reduced to a polynomial term. A common and here also considered approach is to employ

$$W(u) = \alpha u^2(1-u)^2 \quad , \tag{2.15}$$

where the multiplier α controls the influence of the distribution on the total energy. $W(u)$ as defined in (2.15) is plotted in figure 2.6. It is obvious that the double well potential $W(u)$ is minimized by $u = 1$ or $u = 0$, therefore the particles are forced to form clusters, which is expected from the experimental data.

2.3.3 Total energy

So summing up the different energy contribution which are derived in Sections 2.3.1 and 2.3.2 results in the stationary energy of magnetic nanoparticles in a fluid in the presence of an applied

external magnetic field:

$$\begin{aligned} E(u,\mathbf{m}) &= \int_\Omega \frac{\varepsilon_2^2}{2}|\nabla u|^2 + \frac{\varepsilon_4^2}{4}|\nabla u|^4 + W(u) \\ &\quad + \left(A\,|\boldsymbol{\nabla}\mathbf{m}|^2 - J_S \mathbf{H_{ext}} \cdot \mathbf{m} - \frac{1}{2}\mathbf{H_d} \cdot \mathbf{J} \right) \cdot u \; d\mathbf{x} \\ &= \int_\Omega \frac{\varepsilon_2^2}{2}|\nabla u|^2 + \frac{\varepsilon_4^2}{4}|\nabla u|^4 + W(u) + \varepsilon_{mag}^{loc}(\mathbf{m}) \cdot u \; d\mathbf{x} \end{aligned} \tag{2.16}$$

The constraints arising from the model are $|\mathbf{m}| \leq 1$, $0 \leq u \leq 1$ and $\int_\Omega u \, d\mathbf{x} = c_\Omega \cdot |\Omega|$.
The energy functional (2.16) describes the total energy of a closed system at a constant temperature. The second law of thermodynamics states that the energy of such a system will be minimized and the minimum is reached at the state of equilibrium. In the following chapter, the existence of a minimum to this energy functional is shown.

Chapter 3

Mathematical analysis

The energy functional for a ferrofluid under the influence of a magnetic field is derived in the previous chapter. Now a stable state of this system is searched. This is equivalent to the global minimum of the considered energy functional.

This chapter proves the existence of a minimum of the energy functional

$$\begin{aligned} E(u,\mathbf{m}) &= \int_\Omega \frac{\varepsilon^2}{p}|\nabla u|^p \, d\mathbf{x} + \int_\Omega \frac{\varepsilon_2^2}{2}|\nabla u|^2 \, d\mathbf{x} + \int_\Omega W(u) \, d\mathbf{x} \\ &+ \int_\Omega A\,|\boldsymbol{\nabla}\mathbf{m}|^2 \; u \, d\mathbf{x} + \frac{\mu_0}{2}\int_{\mathbb{R}^2} |\nabla V(\mathbf{m})|^2 \; u \, d\mathbf{x} - \int_\Omega J_S \, \mathbf{m}\,\mathbf{H_{ext}} \cdot u \, d\mathbf{x} \end{aligned} \tag{3.1}$$

where u denotes the distribution function of the particles, $\mathbf{m}$ the magnetic polarization vector and $\mathbf{H_{ext}}$ the applied external field, which is bounded by the material dependent saturation magnetization $\mathbf{H_{sat}}$. The argument $\mathbf{m}$ of the scalar stray field potential $V(\mathbf{m})$ is omitted in the following, and further $V_k := V(\mathbf{m}_k)$ is defined. The free energy density $W(u)$ is a nonnegative smooth double well potential, compare equation (2.14). All constants A, ε, ε_2, J_S, μ_0 are positive, and the values are specified in the previous chapter. In the solution space the terms in (3.1) have to be defined. This requirement is met by employing $W^{1,p}(\Omega) \times W^{1,2}(\Omega;\mathbb{R}^2)$. Ω

is assumed to be an open domain with a Lipschitz-continuous boundary, and therefore it is a bounded.

The term $\int_\Omega \frac{\varepsilon_4^2}{4}|\nabla u|^4 \, d\mathbf{x}$, which is introduced in the previous chapter, is substituted by the more general term $\int_\Omega \frac{\varepsilon^2}{p}|\nabla u|^p \, d\mathbf{x}$. In this chapter, the existence of a minimum of the energy functional is proved for all $p > 2$, which obviously includes the case $p = 4$.

The constraints of the distribution function, $0 \leq u(\mathbf{x}) \leq 1$, and of the magnetic polarization, $|\mathbf{m}(\mathbf{x})| \leq 1 \; \forall \mathbf{x} \in \Omega \subset \mathbb{R}^2$, define the constraint sets N_u and $N_\mathbf{m}$:

$$N_u = \{u : \Omega \to \mathbb{R}, \text{ measurable}, \int_\Omega u \, d\mathbf{x} = C_\Omega, \; 0 \leq u \leq 1 \text{ a.e.}\} \quad \Rightarrow \quad \|u\|_{L^\infty} \leq 1 \quad (3.2)$$

$$N_\mathbf{m} = \{\mathbf{m} : \Omega \to \mathbb{R}^2, \text{ measurable}, \; |\mathbf{m}| \leq 1 \text{ a.e.}\} \quad \Rightarrow \quad \|\mathbf{m}\|_{L^\infty} \leq 1 \quad (3.3)$$

Thus

$$X^a = X_u \times X_\mathbf{m} = \left(W^{1,p}(\Omega) \cap N_u\right) \times \left(W^{1,2}(\Omega; \mathbb{R}^2) \cap N_\mathbf{m}\right)$$

is the set of admissible functions. It is obviously a reflexive Banach space for $p > 1$.

Since $W(u)$ is a double well potential, uniqueness of the solution cannot be proved.

Throughout this chapter c is used as a generic constant, which may change from line to line.

3.1 Direct method

Finding the minimizing function to a given functional, where the function has to satisfy certain boundary conditions, is a central issue in the calculus of variations. It arises from many scientific applications. Let

$$\min\{I(w) : w \in X\} \; ,$$

where the functional $I(\cdot)$ is defined as

$$I(w) = \int_\Omega f(\mathbf{x}, w(\mathbf{x}), \nabla w(\mathbf{x})) d\mathbf{x}$$

for $\mathbf{x} \in \Omega \subset \mathbb{R}^n$, $w \in X$, where X is a reflexive Banach space over Ω, and for a continuous function $f : \Omega \times \mathbb{R}^m \times \mathbb{R}^{m\times n}$.

The classical approach to this problem is searching for functions w that solve the first variation $\delta I(w) = 0$. Then the second variation is analyzed for positivity in a neighborhood of these solutions. Thereby many necessary and sufficient conditions have to be studied.

The direct method on the other hand deals with the functional $I(\cdot)$ directly. In the process a minimizing sequence w_k is considered. The convergence of the minimizing sequence and in particular also the existence of a minimum in X has to be guaranteed. Therefore the functional needs to be coercive, i.e. $I(w) \to \infty$ for $\|w\| \to \infty$. If the functional is also sequentially weakly lower semicontinuous, that is

$$I(w_0) \leq \liminf_{k\to\infty} I(w_k),$$

whenever $w_k \rightharpoonup w_0$ weakly in X, then the following theorem, compare e.g. [20], states the existence of a minimum:

Theorem 3.1. *Let X be a reflexive Banach space and $M \subset X$ a sequentially weakly closed subset, $I : M \to \mathbb{R} \cup \{\infty\}$ be a coercive and sequentially weakly lower semicontinuous functional on M. Then $m(I) = \inf_{w\in M} I(w)$ is attained at $w_0 \in M$, i.e. $m(I) = I(w_0)$.*

In the following section, it is proved that the functional $E(\cdot,\cdot)$ as stated in (3.1) fulfills the preconditions of this theorem, and therefore a converging minimizing (sub)sequence exists.

3.2 Coercivity of $E(\cdot,\cdot)$

In this section the coercivity of the considered energy functional $E(\cdot,\cdot)$ is verified.

Proposition 3.2. *The functional $E : X^a \to \mathbb{R}$ as defined in (3.1) is bounded from below and coercive.*

Proof. The functional is bounded from below by $c = -|J_S| \cdot \|\mathbf{H_{ext}}\|_{L^1} > -\infty$, as $\|u\|_{L^\infty}$ and $\|\mathbf{m}\|_{L^\infty}$ are bounded by 1, and each of the remaining integrals is nonnegative:

$$\begin{aligned} E(u,\mathbf{m}) &= \int_\Omega \frac{\varepsilon^2}{p}|\nabla u|^p \, d\mathbf{x} + \int_\Omega \frac{\varepsilon_2^2}{2}|\nabla u|^2 \, d\mathbf{x} + \int_\Omega W(u) \, d\mathbf{x} + \int_\Omega A|\boldsymbol{\nabla}\mathbf{m}|^2 \, u \, d\mathbf{x} \\ &+ \frac{\mu_0}{2}\int_{\mathbb{R}^2} |\nabla V|^2 \, u \, d\mathbf{x} - \int_\Omega J_S \, \mathbf{m}\, \mathbf{H_{ext}} \cdot u \, d\mathbf{x} \\ &\geq -|J_S| \cdot \|u\|_{L^\infty} \|\mathbf{m}\|_{L^\infty} \|\mathbf{H_{ext}}\|_{L^1} \\ &\geq -|J_S| \cdot \|\mathbf{H_{ext}}\|_{L^1} = c \ , \end{aligned}$$

where the constant J_S and the applied external field $\|\mathbf{H_{ext}}\|_{L^1}$ are bounded for physical reasons, see chapter 2.

Let $(u_k)_k$ and $(\mathbf{m}_k)_k$ be sequences in X_u respectively $X_\mathbf{m}$, such that $\|u_k\|_{W^{1,p}} \to \infty$ and $\|\mathbf{m}_k\|_{W^{1,2}} \to \infty$. Since u_k and $\mathbf{m}_k$ are bounded in the considered spaces, it is sufficient to consider $\|\nabla u_k\|_{L^p} \to \infty, \|\boldsymbol{\nabla}\mathbf{m}_k\|_{L^2} \to \infty$. Therefore

$$\begin{aligned} \lim_{\substack{\|\nabla u_k\|\to\infty \\ \|\boldsymbol{\nabla}\mathbf{m}_k\|\to\infty}} E(u_k,\mathbf{m}_k) &= \lim_{\substack{\|\nabla u_k\|\to\infty \\ \|\boldsymbol{\nabla}\mathbf{m}_k\|\to\infty}} \left(\int_\Omega \frac{\varepsilon^2}{p}|\nabla u_k|^p \, d\mathbf{x} + \int_\Omega \frac{\varepsilon_2^2}{2}|\nabla u_k|^2 \, d\mathbf{x} + \int_\Omega W(u_k) \, d\mathbf{x} \right. \\ &+ \left. \int_\Omega A|\boldsymbol{\nabla}\mathbf{m}_k|^2 \, u_k \, d\mathbf{x} + \frac{\mu_0}{2}\int_{\mathbb{R}^2} |\nabla V_k|^2 \, u_k \, d\mathbf{x} - \int_\Omega J_S \, \mathbf{m}_k \, \mathbf{H_{ext}} \cdot u_k \, d\mathbf{x} \right) \\ &\geq \lim_{\substack{\|\nabla u_k\|\to\infty \\ \|\nabla \mathbf{m}_k\|\to\infty}} \left(\int_\Omega \frac{\varepsilon^2}{p}|\nabla u_k|^p \, d\mathbf{x} + \int_\Omega \frac{\varepsilon_2^2}{2}|\nabla u_k|^2 \, d\mathbf{x} \right. \\ &+ \left. \int_\Omega A|\boldsymbol{\nabla}\mathbf{m}_k|^2 \, u_k \, d\mathbf{x} - |J_S| \cdot \|\mathbf{H_{ext}}\|_{L^1} \right) \\ &\longrightarrow \infty \end{aligned}$$

which proves coercivity. □

So $E(\cdot,\cdot)$ is bounded from below and coercive. The following proposition narrows down the space that contains the minimum.

Proposition 3.3. *The minimum of E is contained in a sequentially weakly closed subset $B_r \subset X^a$.*

Proof. Since one is interested in the minimum of the functional, it is sufficient to consider the minimizing sequence $(u_k, \mathbf{m}_k)_k$ only within the subset $B_r = \{(u,\mathbf{m}) : E(u,\mathbf{m}) \leq r\} \subset X^a$, where $r = E(\tilde{u},\tilde{\mathbf{m}})$ and $(\tilde{u},\tilde{\mathbf{m}}) \in X^a$ is arbitrary, such that $B_r \neq \emptyset$. Therefore

$$\min_{(u,\mathbf{m})\in X^a} E(u,\mathbf{m}) = \min_{(u,\mathbf{m})\in B_r} E(u,\mathbf{m}) \quad .$$

It is left to show that the subset B_r is sequentially weakly closed.

The sequence $\phi_k = (u_k, \mathbf{m}_k)$, where $|\mathbf{m}_k| = 1$, converges weakly in $W^{1,p}(\Omega) \times W^{1,2}\left(\Omega;\mathbb{R}^2\right)$, so it converges strongly in $L^p(\Omega) \times L^2\left(\Omega;\mathbb{R}^2\right)$, as $W^{1,p}(\Omega) \times W^{1,2}\left(\Omega;\mathbb{R}^2\right)$ is compactly embedded in $L^p(\Omega) \times L^2\left(\Omega;\mathbb{R}^2\right)$. Because of the strong convergence in $L^p(\Omega) \times L^2\left(\Omega;\mathbb{R}^2\right)$, the sequence converges in measure. This implies the existence of a subsequence $(\phi_{k_n})_{k_n}$ that converges almost everywhere, cf. [22]:

$$\phi_{k_n} \rightharpoonup \phi_0 = (u_0, \mathbf{m}_0) \quad \text{a.e. in} \quad B_r \quad .$$

Thus the subset B_r is sequentially weakly closed and

$$\inf_{(u,\mathbf{m})\in B_r} E(u,\mathbf{m}) = \liminf_{k_n\to\infty} E(u_{k_n}, \mathbf{m}_{k_n})$$

□

3.3 Weak sequential lower semicontinuity

In the previous section we proved that the minimum of the energy functional $E(\cdot,\cdot)$ is obtained in a sequentially weakly closed subset, so it is sufficient to consider only a minimizing sequence

$(u_k, \mathbf{m}_k)_k \subset B_r$, such that $E(u_k, \mathbf{m}_k)$ is bounded by r. If the functional is also sequentially weakly lower semicontinuous on B_r, then theorem 3.1 states the existence of a minimum in B_r.

Proposition 3.4. *The functional $E : X^a \to \mathbb{R}$ as defined in (3.1) is sequentially weakly lower semicontinuous.*

Proof. Since $\mathbf{H_{ext}}$, u and $\mathbf{m}$ are bounded, (3.1) becomes

$$\begin{aligned} E(u,\mathbf{m}) &\geq \int_\Omega \frac{\varepsilon^2}{p}|\nabla u|^p \, d\mathbf{x} + \int_\Omega \frac{\varepsilon_2^2}{2}|\nabla u|^2 \, d\mathbf{x} + \int_\Omega W(u) \, d\mathbf{x} \\ &+ A\int_\Omega |\boldsymbol{\nabla}\mathbf{m}|^2 \, u \, d\mathbf{x} + \frac{\mu_0}{2}\int_{\mathbb{R}^2} |\nabla V|^2 \, u \, d\mathbf{x} - \overbrace{|J_S| \, \|\mathbf{m}\|_{L^\infty} \, \|u\|_{L^\infty} \, \|\mathbf{H_{ext}}\|_{L^1}}^{=c>0} \\ r + c &\geq \int_\Omega \frac{\varepsilon^2}{p}|\nabla u|^p \, d\mathbf{x} + \int_\Omega \frac{\varepsilon_2^2}{2}|\nabla u|^2 \, d\mathbf{x} + \int_\Omega W(u) \, d\mathbf{x} \\ &+ \int_\Omega A|\boldsymbol{\nabla}\mathbf{m}|^2 \, u \, d\mathbf{x} + \frac{\mu_0}{2}\int_{\mathbb{R}^2} |\nabla V|^2 \, u \, d\mathbf{x} \quad . \end{aligned} \tag{3.4}$$

Since every summand on the right hand side is nonnegative, each summand is also bounded. As $W(u)$ is a smooth function, it is sequentially lower semicontinuous. The norm is also weakly sequentially lower semicontinuous, thus for the first three terms sequential lower semicontinuity is proved:

$$\begin{aligned} \liminf_{k\to\infty} &\left(\int_\Omega \frac{\varepsilon^2}{p}|\nabla u_k|^p \, d\mathbf{x} + \int_\Omega \frac{\varepsilon_2^2}{2}|\nabla u_k|^2 \, d\mathbf{x} + \int_\Omega W(u_k) \, d\mathbf{x} \right) \\ &\geq \int_\Omega \frac{\varepsilon^2}{p}|\nabla u_0|^p \, d\mathbf{x} + \int_\Omega \frac{\varepsilon_2^2}{2}|\nabla u_0|^2 \, d\mathbf{x} + \int_\Omega W(u_0) \, d\mathbf{x} \end{aligned}$$

Following theorem and lemma are needed to verify lower semicontinuity of the two terms $\int_\Omega |\boldsymbol{\nabla}\mathbf{m}_k|^2 \, u_k \, d\mathbf{x}$ and $\int_{\mathbb{R}^2} |\nabla V_k|^2 \, u_k \, d\mathbf{x}$. Compact embedding is denoted by $\hookrightarrow\hookrightarrow$.

Theorem 3.5. *Let $\Omega \subset \mathbb{R}^n$ be an open domain with a Lipschitz-continuous boundary, $n \geq 2$, $p \in [1, \infty[$, $k \in \mathbb{N}$, $kp > n$. Then*

$$W^{k,p}(\Omega) \hookrightarrow\hookrightarrow C(\overline{\Omega}).$$

See e.g. reference [23].

As $k = 1$ and $n = 2$ are considered, the assumption $p > 2$ is sufficient for the application of the theorem. Then

$$u_k \rightharpoonup u_0 \text{ in } W^{1,p} \Rightarrow u_k \to u_0 \text{ in } C(\overline{\Omega})$$

$$\sup_{\overline{\Omega}} |u_k - u_0| \to 0$$

Lemma 3.6. *Let $(u_k)_k$ in $W^{1,p}(\Omega)$, $p > n$, where $\Omega \subset \mathbb{R}^n$. Let $(f_k)_k$ in $L^2(\Omega; \mathbb{R}^d)$ and $f_k \rightharpoonup f_0$ weakly. Then*

$$\liminf_{k\to\infty} \int_\Omega |f_k|^2 u_k \, d\mathbf{x} \geq \int_\Omega |f_0|^2 u_0 \, d\mathbf{x} \tag{3.5}$$

Proof. As a beginning, the term $u_0 - u_0$ is added to u_k and the integral is divided into two parts

$$\int_\Omega |f_k|^2 u_k \, d\mathbf{x} = \int_\Omega |f_k|^2 u_0 \, d\mathbf{x} + \underbrace{\int_\Omega \overbrace{|f_k|^2}^{\in L^1} \overbrace{(u_k - u_0)}^{\in L^\infty} \, d\mathbf{x}}_{(*)}$$

Then only the second integral is considered

$$|(*)| \leq \|f_k\|_{L^2}^2 \cdot \|u_k - u_0\|_{L^\infty} \leq c\|u_k - u_0\|_{L^\infty}$$

As $(u_k)_k$ in $W^{1,p}(\Omega)$, $u_k \to u_0$ in $C(\bar{\Omega})$

$$\lim_{k\to\infty} \|u_k - u_0\|_{L^\infty} \to 0 \text{ in } C(\bar{\Omega}) \Rightarrow \lim_{k\to\infty} (*) = 0 \tag{3.6}$$

So

$$\lim_{k\to\infty} \int_\Omega |f_k|^2 u_k \, d\mathbf{x} = \lim_{k\to\infty} \int_\Omega |f_k|^2 u_0 \, d\mathbf{x} = \lim_{k\to\infty} \int_\Omega |f_k \sqrt{u_0}|^2 \, d\mathbf{x} \tag{3.7}$$

Since $u_0 \in L^2(\Omega)$ and continuous, also $\sqrt{u_0} \in L^2(\Omega)$. Having $f_k \rightharpoonup f_0$ weakly in $L^2(\Omega; \mathbb{R}^d)$ results in the weak convergence $f_k\sqrt{u_0} \rightharpoonup f_0\sqrt{u_0}$ in $L^2(\Omega; \mathbb{R}^d)$.

The norm is sequentially weakly lower semicontinuous, therefore

$$\begin{aligned}\liminf_{k\to\infty}\int_\Omega |f_k|^2 u_k \; d\mathbf{x} &= \liminf_{k\to\infty}\int_\Omega |f_k|^2 u_0 \; d\mathbf{x} = \liminf_{k\to\infty} \|f_k\sqrt{u_0}\|_{L^2}^2 \\ &\geq \|f_0\sqrt{u_0}\|_{L^2}^2\end{aligned}$$

□

It is left to show that $(\boldsymbol{\nabla}\mathbf{m}_k)_k$ and $(\nabla V_k)_k$ satisfy the assumptions of lemma (3.6), which implies sequential lower semicontinuity of the energy functional (3.1).

Proposition 3.7. *$(\boldsymbol{\nabla}\mathbf{m}_k)_k$ in $L^2(\Omega;\mathbb{R}^4)$ and $\boldsymbol{\nabla}\mathbf{m}_k \rightharpoonup \boldsymbol{\nabla}\mathbf{m}_0$ weakly in $L^2(\Omega;\mathbb{R}^4)$.*

Proof. Since $(\mathbf{m}_k)_k$ in $W^{1,2}\left(\Omega;\mathbb{R}^2\right)$, obviously $(\boldsymbol{\nabla}\mathbf{m}_k)_k$ in $L^2(\Omega;\mathbb{R}^4)$, compare A.1.
The boundedness of $(\boldsymbol{\nabla}\mathbf{m}_k)_k$ is necessary to prove the weak sequential convergence. Therefore an arbitrary small, positive lower bound on u_k is considered: $0 < \delta \leq u_k \leq 1$. Then

$$\begin{aligned}\int_\Omega \delta|\boldsymbol{\nabla}\mathbf{m}_k|^2 \; d\mathbf{x} \leq \int_\Omega u_k|\boldsymbol{\nabla}\mathbf{m}_k|^2 \; d\mathbf{x} \leq c \\ \Rightarrow \; \|\boldsymbol{\nabla}\mathbf{m}_k\|_{L^2(\Omega)}^2 \leq \frac{c}{\delta} \quad ,\end{aligned}$$

where the upper bound of $\int_\Omega |\boldsymbol{\nabla}\mathbf{m}_k|^2 u_k \; d\mathbf{x}$ follows from the constraint (3.4). □

Proposition 3.8. *$(\nabla V_k)_k$ in $L^2(\mathbb{R}^2;\mathbb{R}^2)$ and $\nabla V_k \rightharpoonup \nabla V_0$ weakly in $L^2(\mathbb{R}^2;\mathbb{R}^2)$.*

Proof. V_k depends on $\mathbf{m}_k$ as

$$\frac{J_S}{\mu_0}\mathrm{div}(\chi_\Omega \mathbf{m}_k) = \Delta V_k \qquad \Rightarrow \qquad V_k = \Delta^{-1}\left(\frac{J_S}{\mu_0}\chi_\Omega \mathrm{div}\; \mathbf{m}_k\right) \quad .$$

Since $\mathbf{m}_k \in W^{1,2}(\Omega;\mathbb{R}^2)$, div $\mathbf{m}_k \in L^2(\Omega)$, compare A.1, and expanded to the whole space div $(\chi_\Omega \mathbf{m}_k) \in L^2(\mathbb{R}^2)$, from which it follows $(V_k)_k$ in $W^{1,2}(\mathbb{R}^2)$.
Therefore $(V_k)_k = \left(\Delta^{-1}\left(\frac{J_S}{\mu_0}\mathrm{div}\chi_\Omega \mathbf{m}_k\right)\right)_k$ converges weakly in $W^{1,2}(\mathbb{R}^2)$ and $(\nabla V_k)_k$ con-

verges weakly in $L^2(\mathbb{R}^2;\mathbb{R}^2)$. $(\nabla V)_k$ is bounded as

$$\begin{aligned}
&\frac{\mu_0}{2}\int\limits_{\mathbb{R}^2}|\nabla V_k|^2\ d\mathbf{x} = \frac{\mu_0}{2}\|\nabla V_k\|^2_{L^2(\mathbb{R}^2)} \geq \frac{\mu_0}{2}\|\nabla V_k\|^2_{L^2(\Omega)} \quad \text{and}\\
&\frac{\mu_0}{2}\int\limits_{\mathbb{R}^2}|\nabla V_k|^2\ d\mathbf{x} = \frac{J_S}{2}\int\limits_{\Omega}\mathbf{m}_k|\nabla V_k|\ d\mathbf{x} \leq \frac{J_S}{2}\|\mathbf{m}_k\|_{L^2(\Omega)}\|\nabla V_k\|_{L^2(\Omega)}\\
\Rightarrow\quad &\|\nabla V_k\|_{L^2(\Omega)} \leq \frac{J_S}{\mu_0}\|\mathbf{m}_k\|_{L^2(\Omega)} \leq c
\end{aligned}$$

□

At last the sequential lower semicontinuity of $f = -\int_\Omega J_S\,\mathbf{H_{ext}}\mathbf{m}\ u\ d\mathbf{x}$ is proved. Since the convergence $u_k \to u_0$ in $L^p(\Omega) \subset L^2(\Omega)$ and $\mathbf{m}_k \to \mathbf{m}_0$ in $L^2(\Omega;\mathbb{R}^2)$ are strong, the term is continuous in u and $\mathbf{m}$ and therefore

$$\liminf_{k\to\infty}\left(-\int\limits_{\Omega}J_S\,\mathbf{H_{ext}}\mathbf{m}_k\ u_k\ d\mathbf{x}\right) = -\int\limits_{\Omega}J_S\,\mathbf{H_{ext}}\mathbf{m}_0\ u_0\ d\mathbf{x} \tag{3.8}$$

So each summand of the functional $E(u,\mathbf{m})$ is lower semicontinuous and therefore the functional overall. □

3.4 Conclusion

In the two previous sections, it was proved that the considered energy functional as defined in 3.1 is coercive, lower semicontinuous and attains its minimum on a sequentially weakly closed subset if the additional restrictions $0 < \delta \leq u$ and $p > n$ are assumed. Then theorem 3.1 holds and therefore we can indeed conclude that a minimum $(u_0,\mathbf{m}_0)$ of the functional $E(\cdot,\cdot)$ exists in the considered reflexive Banach space X^a:

$$\begin{aligned}
E(u_0,\mathbf{m}_0) &= \inf_{(u,\mathbf{m})\in X^a} E(u,\mathbf{m}) = \inf_{(u,\mathbf{m})\in B_r} E(u,\mathbf{m})\\
&= \liminf_{k_n\to\infty} E(u_{k_n},\mathbf{m}_{k_n}) \geq E(u_0,\mathbf{m}_0)
\end{aligned}$$

Chapter 4

Simulation

This chapter shows and discusses the simulation results of the pattern formed by magnetic nanoparticles on a surface under the influence of an applied external magnetic field. The model is derived in Chapter 2, the existence of a solution is proved in Chapter 3.

As a start, the considered problem is restated and additional boundary conditions, which are necessary for the numerical simulation, are established in Section 4.1. Then the equation is discretized and the generation of the mesh is approached in Section 4.2. The resulting problem is solved by means of global optimization. The basics of this method are outlined in Section 4.3, where also the most important algorithms for global nonlinear optimization are introduced. Section 4.4 discusses the numerical results.

4.1 Model

Consider the domain $\Omega \subset \mathbb{R}^2$ to be occupied by the ferrofluid. It is given the following problem

$$\begin{aligned} \min_{(u,\mathbf{m})\in X^a} E(u,\mathbf{m}) &= \min_{(u,\mathbf{m})\in X^a} \int_\Omega \frac{\varepsilon_4^2}{4}|\nabla u|^4 + \frac{\varepsilon_2^2}{2}|\nabla u|^2 + \alpha u^2(1-u)^2 \\ &\quad + \left(A\,|\boldsymbol{\nabla}\mathbf{m}|^2 - J_S\,\mathbf{H_{ext}}\cdot\mathbf{m} + \frac{1}{2}J_S\,\nabla V\cdot\mathbf{m}\right)\cdot u\; d\mathbf{x} \\ &= \min_{(u,\mathbf{m})\in X^a} \int_\Omega \frac{\varepsilon_4^2}{4}|\nabla u|^4 + \frac{\varepsilon_2^2}{2}|\nabla u|^2 + W(u) + \varepsilon_{mag}^{loc}(\mathbf{m})\cdot u\; d\mathbf{x} \end{aligned} \tag{4.1}$$

where the minimum of the free energy functional E is searched over a particle distribution u and a magnetic direction vector $\mathbf{m}$. The constraints arising from the model are the following: the magnetic direction vector has the maximal length one, i.e. $|\mathbf{m}| \leq 1$, the distribution u is between $0 \leq u \leq 1$, and the concentration of particles in Ω is fixed such that $\int_\Omega u\,d\mathbf{x} = C_\Omega$. Therefore the feasible set X^a is given by

$$\begin{aligned} N_u &= \{u : \Omega \to \mathbb{R},\ \text{measurable}, 0 \leq u \leq 1 \text{ a.e.},\ \text{ and } \int_\Omega u\,d\mathbf{x} = C_\Omega\} \\ N_{\mathbf{m}} &= \{\mathbf{m} : \Omega \to \mathbb{R}^2,\ \text{measurable},\ |\mathbf{m}| \leq 1 \text{ a.e.}\} \\ X^a &= \left(W^{1,4}(\Omega)\cap N_u\right) \times \left(W^{1,2}(\Omega;\mathbb{R}^2)\cap N_{\mathbf{m}}\right)\ . \end{aligned} \tag{4.2}$$

$\mathbf{J} = J_S \cdot \mathbf{m}$ denotes the local magnetic polarisation vector. The stray field energy is given by $\mathbf{H_d} = -\nabla V$, where the potential V is given by the equation

$$\Delta V = \text{div}\ (\chi_\Omega \mathbf{m}) \qquad \text{on}\ \ \mathbb{R}^2\ \ . \tag{4.3}$$

The applied external field $\mathbf{H_{ext}}$ is assumed to be homogeneous over the considered domain.

4.1.1 Boundary conditions

For simulation boundary conditions are necessary for the variables u, $\mathbf{m}$ and also for the potential V. Dirichlet boundary conditions are considered for u. The boundary of Ω is denoted

by Γ. Neumann boundary conditions are assumed for the magnetic field.

As stated above, the magnetic potential V is defined at the whole plane $\mathbb{R}^2$. It approaches zero at infinity. In micromagnetism, two methods exist for the evaluation of equation (4.3): In this thesis, V is evaluated on a compact subset $\tilde{\Omega}$, where $\Omega \Subset \tilde{\Omega} \subset \mathbb{R}^2$. According to [25] $diam\ \tilde{\Omega} \approx 10 \cdot diam\ \Omega$ suffices to capture relevant magnetostatic energy contribution. The potential V is constant on the boundary of $\tilde{\Omega}$, therefore $V = 0$ is considered without loss of generality, compare [26].

The second approach, which is discussed e.g. in [27], defines a convolution operator $\mathcal{L}$ with a Newtonian kernel G such that

$$V := \mathcal{L}\mathbf{m} := \sum_{j=1}^{d} \frac{\partial G}{\partial x_j} * m_j \quad .$$

This approach holds for any arbitrary smooth magnetization $\mathbf{m} = (m_1, ..., m_d)$. This thesis considers $\mathbf{m} \in W^{1,2}(\Omega; \mathbb{R}^2)$, so smoothness of $\mathbf{m}$ is not guaranteed. Since the method of truncating $\mathbb{R}^2$ to $\tilde{\Omega}$ shows good results, the convolution operator is not further studied.

The boundary of $\tilde{\Omega}$ is denoted by Γ_V, further $\tilde{\Omega}$ is partitioned in the closed domains Ω and Ω_V, which share the boundary Γ such that $\Gamma = \Omega \cap \Omega_V$ and $\tilde{\Omega} = \Omega \cup \Omega_V$, see figure 4.1.

Summarizing the constraints

$$u \leq 1 \tag{4.4}$$

$$-u \leq 0 \tag{4.5}$$

$$\|\mathbf{m}\|_{L^2} \leq 1 \tag{4.6}$$

$$\int u\, dx = C_\Omega \tag{4.7}$$

$$u = 0 \quad \text{on } \Gamma \tag{4.8}$$

$$\frac{\partial \mathbf{m}}{\partial \mathbf{n}} = 0 \quad \text{on } \Gamma \tag{4.9}$$

$$V = 0 \quad \text{on } \Gamma_V \quad , \tag{4.10}$$

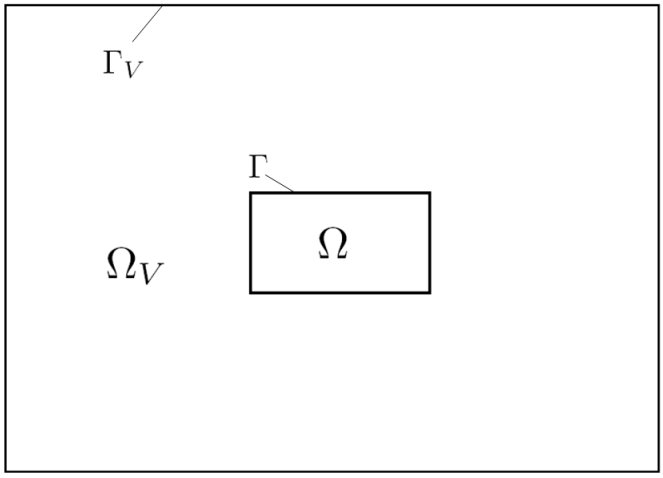

Figure 4.1: Sketch of the domains Ω and Ω_V. The boundary Γ belongs to both domains: $\Gamma = \Omega \cap \Omega_V$.

where all constraints are linear except constraint (4.6). Be X the set of all feasible points $(u, \mathbf{m})$ that satisfy these constraints.

$$X := \left\{ (u, \mathbf{m}) \in \left(W^{1,4}(\Omega) \times W^{1,2}(\Omega; \mathbb{R}^2) \right) \ : \ \text{constraints } (4.4) - (4.10) \ \text{ hold } \right\}$$

The set X is obviously convex.

4.2 Discretization

Problem (4.1) is solved numerically, therefore it is discretized. Thus the solution is not obtained in the infinite dimensional space X but it is approximated in a suitable finite dimensional subspace X_h. In Section 4.2.1 the triangulation of domains Ω and Ω_V is defined, and in Section 4.2.2 the equation is discretized over this mesh using finite element methods and X_h is specified.

4.2.1 Triangulation

It is assumed that the domains Ω and Ω_V are open polygonal plane domains with a Lipschitz-boundary, compare Chapter 3. Below, the triangulation is defined for Ω but of course it holds for Ω_V analogously. The expression 'triangulation' is commonly used for all kinds of mesh, not only for triangles. Throughout this thesis, discretization by triangles is used.

Definition 4.1. *Be $\mathcal{T}_h$ a triangulation of Ω such that Ω is divided into subsets or elements K. These elements K of a feasible triangulation satisfy following three conditions:*

1. $\bar{\Omega} = \bigcup_{K \in \mathcal{T}_h} K$
2. *int* $K_1 \cap$ *int* $K_2 = \emptyset$ *holds for each distinct* K_1, $K_2 \in \mathcal{T}_h$
3. *Every face of any element $K_1 \in \mathcal{T}_h$ is either a face of another element $K_2 \in \mathcal{T}_h$ or part of the boundary $\partial\Omega = \Gamma$. The boundary is covered by the boundaries of the elements.*

The discretization or triangulation parameter $h > 0$ quantifies the maximal diameter of all elements $K \in \mathcal{T}_h$. It characterizes the maximal length of an edge in the case of triangles. For a given sufficient small parameter h there exist several different triangulations $\mathcal{T}_h$ of Ω.

Definition 4.2. *The triangulation $\mathcal{T}_h$ is regular if one of the following conditions is met:*

1. $\exists\ c > 0$ *such that the area of each triangle K is bounded from below by ch^2,*
2. $\exists\ m > 0$ *such that every triangle K is contained in a ball of radius h and contains a ball of radius mh,*
3. *the minimum angle of each triangle is bounded from below by some constant > 0,*

and all constants are independent of h.

The vertices of the triangles are called nodes.

When speaking of triangulation, this thesis always refers to a triangulation that satisfies both definitions 4.1 and 4.2. Therefore also the triangular mesh used for calculation satisfies both definitions. It is generated by the freeware finite element mesh generator gmsh [28].

4.2.2 Finite element discretization

The task of finding a solution of problem (4.1) in the infinite dimensional space X over the domain Ω is now replaced by finding an approximate solution of the problem in a finite dimensional subspace X_h. Be $\mathbf{x}_j,\ j = 1...N$, the nodes of the triangulation, where N denotes the total number of nodes. Then in this thesis X_h is an approximate N-dimensional subspace that is spanned on behalf of piecewise linear basis function η_j which have a compact support and $\eta_i(\mathbf{x}_j) = \delta_{ij}$ for $i, j = 1...N$.

The distribution function u and the magnetization vector $\mathbf{m}$ are approximated in X_h by a linear combination of the global basis functions such that

$$u_h(\mathbf{x}) = \sum_{j=1}^{N} u_j \cdot \eta_j(\mathbf{x}) \qquad \text{and} \qquad \mathbf{m}_h(\mathbf{x}) = \sum_{j=1}^{N} \mathbf{m}_j \cdot \eta_j(\mathbf{x}) \quad . \tag{4.11}$$

Now let (x_1, y_1), (x_2, y_2) and (x_3, y_3) be the vertices of a triangular element K. Then locally the linear basis functions are given by

$$\eta_j(x,y) = \frac{1}{T_z} \det \begin{pmatrix} 1 & x & y \\ 1 & x_{j+1} & y_{j+1} \\ 1 & x_{j+2} & y_{j+2} \end{pmatrix} , \quad \text{where}$$

$$T_z = \det \begin{pmatrix} 1 & x_j & y_j \\ 1 & x_{j+1} & y_{j+1} \\ 1 & x_{j+2} & y_{j+2} \end{pmatrix} = 2 \cdot \int_K 1 \; d\mathbf{x}$$

and the indices are modulo 3.

Using this basis functions, u and $\mathbf{m}$ are replaced in problem (4.1) by their piecewise linear approximations (4.11). This replacement allows for elementwise integration, which is calculated in appendix B.

The result is a nonlinear equation system in the $3 \cdot N$ unknowns u_i, m_{1i} and m_{2i}, where $i = 1...N$ and $\mathbf{m}_i = (m_{1i}, m_{2i})^T$. This system is denoted by $f(\mathbf{y})$, where $\mathbf{y} = (\mathcal{U}, \mathcal{M}_1, \mathcal{M}_2)^T$ and $\mathcal{U} = (u_1, ..., u_N)$, $\mathcal{M}_1 = (m_{1,1}, ..., m_{1,N})$ and $\mathcal{M}_2 = (m_{2,1}, ..., m_{2,N})$. Also the constraints (4.4)-(4.10) are discretized. The resulting t equality constraints $h_i(\mathbf{y})$ are combined in one t-dimensional vector such that $\mathbf{h}(\mathbf{y}) = \mathbf{0}$ and the m inequality constraints $g_i(\mathbf{y})$ are combined such that $\mathbf{g}(\mathbf{y}) \leq \mathbf{0}$.

Therefore the discrete form of problem (4.1) is given by

$$\begin{aligned} \min_{\mathbf{y}} \quad & f(\mathbf{y}) \\ \text{subject to} \quad & \mathbf{h}(\mathbf{y}) = \mathbf{0} \\ & \mathbf{g}(\mathbf{y}) \leq \mathbf{0} \end{aligned} \tag{4.12}$$

4.3 Global Optimization

Problem (4.1) is clearly nonlinear therefore also the discretized problem (4.12). The task is to find the global minimum of a nonlinear optimization problem where the constraints are convex. There exists no general algorithm to find definitely the global optimum of a given problem. If a suitable starting vector, that is close enough to the expected global solution, is used, local optimization methods provide for global optimal points.

This section starts by explaining the basic concepts of nonlinear constrained optimization in Section 4.3.1 and continues by outlining the used algorithms in Section 4.3.2.

4.3.1 Basics: nonlinear constrained optimization problem

The standard format of a nonlinear constrained optimization problem with a merit, objective or target function $f : \mathbb{R}^n \to \mathbb{R}$, inequality constraint $\mathbf{g} : \mathbb{R}^n \to \mathbb{R}^m$, where $\mathbf{g}(\mathbf{y}) = (g_1(\mathbf{y}), ..., g_m(\mathbf{y}))^T$, and equality constraint $\mathbf{h} : \mathbb{R}^n \to \mathbb{R}^t$, where $\mathbf{h}(\mathbf{y}) = (h_1(\mathbf{y}), ..., h_t(\mathbf{y}))^T$, is given by

$$\begin{aligned} \min_{\mathbf{y}} \quad & f(\mathbf{y}) \\ \text{subject to} \quad & \mathbf{g}(\mathbf{y}) \leq \mathbf{0}, \\ & \mathbf{h}(\mathbf{y}) = \mathbf{0}. \end{aligned} \tag{4.13}$$

The dimension of the zero vector $\mathbf{0}$ is chosen according to the dimension of the (in)equality. The problem treated in this thesis, problem (4.12), is obviously contained in this formulation when $\mathbf{y} = (u, \mathbf{m})$. The here considered functions are also all clearly continuously differentiable at all $\mathbf{y} \in X$. The Fréchet derivative of the objective function f at $\mathbf{y}$, $Df(\mathbf{y})$ in short, is given by

$$Df(\mathbf{y})\mathbf{v} = \int_\Omega \begin{pmatrix} -\varepsilon_4^2 \nabla \left(|\nabla u|^2 \nabla u \right) - \varepsilon_2^2 \Delta u + 2\alpha \left(u - 3u^2 + 2u^3 \right) + \varepsilon_{mag}^{loc}(\mathbf{m}) \\ -2A \nabla (u \boldsymbol{\nabla} \mathbf{m}) - \left(\mathbf{H_{ext}}\, J_S + \frac{1}{2} J_S\, \nabla V \right) \cdot u \end{pmatrix} \cdot \mathbf{v}\; d\mathbf{x} \tag{4.14}$$

The equality constraint in equation (4.13) could be transformed to two inequality constraints:

$$\begin{aligned} \mathbf{h}(\mathbf{y}) &\leq \mathbf{0} \\ -\mathbf{h}(\mathbf{y}) &\leq \mathbf{0}. \end{aligned} \tag{4.15}$$

Therefore, theoretical considerations are restricted to inequality constraints without loss of generality. For computation, it is recommended to deal with problem (4.13) as the number of constraints and the condition of the problem is increased by using (4.15) instead of $\mathbf{h}(\mathbf{y}) = \mathbf{0}$.

Karush-Kuhn-Tucker equation, Lagrange Multipliers

The constrained optimization problem (4.13) is reformulated by means of Lagrange multipliers $\boldsymbol{\mu} = (\mu_1, ..., \mu_m)$ and $\boldsymbol{\lambda} = (\lambda_1, ..., \lambda_t)$ as an unconstrained optimization problem $\mathcal{L}(\mathbf{y}, \boldsymbol{\mu}, \boldsymbol{\lambda})$, which can be easily solved, e.g. by a gradient method.

$$\mathcal{L}(\mathbf{y}, \boldsymbol{\mu}, \boldsymbol{\lambda}) = f(\mathbf{y}) + \sum_{i=1}^{m} \mu_i g_i(\mathbf{y}) + \sum_{j=1}^{t} \lambda_j h_j(\mathbf{y}) \tag{4.16}$$

Be f, $\mathbf{g}$ and $\mathbf{h}$ continuously differentiable at the feasible point $\bar{\mathbf{y}}$. This condition is fulfilled by the here considered function, see (4.14). Define the set of active inequality constraints

$$\mathcal{I}(\mathbf{y}) := \{i \in \{1...m\} : g_i(\mathbf{y}) = 0\}.$$

Problem (4.13) satisfies the linear independence constraint qualification (LICQ) condition at a point $\mathbf{y}$, if the gradients of the equality constraints $\nabla h_j(\mathbf{y})$, $j = 1...t$, and of the active inequality constraints $\nabla g_i(\mathbf{y})$, $i \in \mathcal{I}(\mathbf{y})$, are linearly independent. There exist different constraint qualifications that follow from the LICQ condition. One of them might replace the LICQ condition in the following statement, but some constraint qualifications hold only for special cases of problem (4.13).

If $\bar{\mathbf{y}}$ is a minimal point where the LICQ condition is satisfied, there exist constants $\boldsymbol{\mu}$ and $\boldsymbol{\lambda}$ such that the Karush-Kuhn-Tucker (KKT) conditions (4.17)-(4.18) are satisfied. First, the point is stationary

$$\nabla_{\mathbf{y}} \mathcal{L}(\bar{\mathbf{y}}, \boldsymbol{\mu}, \boldsymbol{\lambda}) = \nabla f(\bar{\mathbf{y}}) + \sum_{i=1}^{m} \mu_i \nabla g_i(\bar{\mathbf{y}}) + \sum_{j=1}^{t} \lambda_j \nabla h_j(\bar{\mathbf{y}}) \quad = \quad \mathbf{0} \tag{4.17}$$

then the primal feasibility

$$\mathbf{g}(\bar{\mathbf{y}}) \quad \leq \quad \mathbf{0}$$

$$\mathbf{h}(\bar{\mathbf{y}}) \quad = \quad \mathbf{0}$$

and the dual feasibility

$$\boldsymbol{\mu} \geq \mathbf{0}$$

are satisfied. Finally the complementary slackness condition

$$\boldsymbol{\mu}^T \mathbf{g}(\bar{\mathbf{y}}) = \mathbf{0} \tag{4.18}$$

holds.

Barrier function

In order to assure that the constraints are satisfied in computation, a barrier or a penalty function is added to the objective function. It is described in terms of inequality-constrained optimization problems. Equality constraints are according to equation (4.15) transformable to inequality constraints. Therefore without loss of generality the barrier function is defined only for inequality constrained problems.

Be $\mathbf{c}(x) = (c_1(x), ..c_m(x))^T$. Given the problem

$$\begin{aligned} \min_x \quad & f(x) \\ \text{subject to} \quad & \mathbf{c}(x) \leq \mathbf{0} \quad . \end{aligned} \tag{4.19}$$

Be X the feasible set of (4.19)

$$X := \{ x \in \mathbb{R}^n \mid \mathbf{c}(x) \leq \mathbf{0} \} \ . \tag{4.20}$$

The inequality constraints $\mathbf{c}(x) \leq 0$ are transformed by means of positive slack variables $\mathbf{s} = (s_1, ...s_m)^T$ to equality constraints

$$\begin{aligned} \min_x \quad & f(x) \\ \text{subject to} \quad & \mathbf{c}(x) + \mathbf{s} = \mathbf{0}, \\ & \mathbf{s} \geq \mathbf{0} \quad , \end{aligned} \tag{4.21}$$

since equality constrained problems are easier to solve.

The feasible set S of problem (4.21) has the form

$$S := \left\{ (x, \mathbf{s}) \in X \times \mathbb{R}^m_+ \mid \mathbf{c}(x) = -\mathbf{s}, \ \mathbf{s} \geq \mathbf{0} \right\} \ ,$$

and the strictly feasible set S^0 of problem (4.21) is defined as

$$S^0 := \left\{ (x, \mathbf{s}) \in X \times \mathbb{R}^m_+ \mid \mathbf{c}(x) = -\mathbf{s},\ \mathbf{s} > \mathbf{0} \right\} .$$

It is assumed that S^0 is nonempty.

Definition 4.3. *A barrier function for problem (4.21) satisfies following properties*

- *It is smooth inside* S^0 ,
- *it is infinitely everywhere except in* S^0 *and*
- *its value approaches* ∞ *as* $\mathbf{s}$ *approaches the boundary of* S^0.

A barrier function $\phi(\xi)$ *is said to be of the order* λ *if* ϕ' *has a pole of order* λ *at* $\xi = 0$.

The logarithm is a common choice as a barrier function. It satisfies all three properties above. It is of order 1. For the given constraint set $\mathbf{s}_i \geq 0$, $i = 1...m$, the logarithmic barrier function is given by

$$-\sum_{i=1}^{m} \ln(s_i) .$$

Using this barrier function, an approximate problem to problem (4.21) is formulated

$$\begin{aligned} & \min_{(x,\mathbf{s})} f_\sigma(x, \mathbf{s}) = \min_{(x,\mathbf{s})} \left(f(x) - \sigma \sum_{i=1}^{m} \ln(s_i) \right) \\ \text{subject to} \quad & \mathbf{c}(x) + \mathbf{s} = \mathbf{0}, \\ & \mathbf{s} \geq \mathbf{0} \quad , \end{aligned}$$

where $\sigma > 0$ is the barrier parameter. The functions $-\sigma \ln(s_i)$ create a barrier close to the boundary of S^0 where they increase to ∞. Therefore the values of the functions s_i are prevented from getting too close to this boundary.

The barrier parameter σ is gradually decreased to 0, and then the solution converges to a

solution of the original problem - if certain conditions are satisfied. These conditions are given by lemma 4.4 and theorem 4.5, compare [30].

The corresponding Lagrangian is

$$\mathcal{L}(x, \mathbf{s}, \boldsymbol{\mu}, \boldsymbol{\lambda}) = f(x) - \sigma \sum_{i=1}^{m} \mu_i \ln(s_i) + \sum_{i=1}^{m} \mu_i \left(c_i(x) + s_i\right)$$

The existence of a feasible starting point x_s that satisfies $\mathbf{g}(x_s) < \mathbf{0}$ is necessary for the existence of a feasible solution for all $\sigma > 0$. Following lemma, compare [30], states this condition:

Lemma 4.4. *Assume that the feasible set of problem (4.13) is bounded. Then for every $\sigma > 0$ problem (4.22) has a solution $(x(\sigma), \mathbf{s}(\sigma))$.*

Note that the feasible set S^0 is nonempty since $(x_s, -\mathbf{c}(x_s))$ belongs to S^0.

Observe that S is the closure of S^0 and the entire feasible set of problem (4.21).

Then following theorem holds:

Theorem 4.5. *Assume that the feasible set of problem (4.13) is bounded and S is satisfied. If $\sigma_k \to 0$ as $k \to \infty$, then every accumulation point of the sequence $(x(\sigma_k), \mathbf{s}(\sigma_k))$ is a solution of problem (4.21).*

Merit function

Adding one penalty term for each constraint to the objective function is another method to eliminate the constraints. The penalty term is positive, if the constraint is violated, and zero otherwise. The resulting new objective function is called penalty or merit function. Often, a sequence of merit functions is considered, where the penalty coefficients grow at each iteration an therefore constraint violations are penalized more severely.

If the interior point algorithm takes a conjugate gradient step, the step size and direction are chosen such that a merit function is minimized, see section below.

4.3.2 Algorithms

Matlab provides three algorithms for calculation, which are the most important optimization algorithms: `trust-region-reflective`, `interior-point` and `active-set`. Since the considered problem is a large-scale problem and the `trust-region-reflective` is only suitable for small-scale problems, only the latter two algorithms are appropriate for the considered problem. In the following they are introduced, whereas the in Matlab implemented models are emphasized, which are outlined in [31].

Interior-point algorithm

The interior-point algorithm solves constrained minimization problems by using a sequence of approximate minimization problems. These approximate problems are generated by applying a barrier function. They are solved either by taking a direct - also called Newton - step or by taking a conjugate gradient step.

Barrier function Adding slack variables and the logarithmic barrier function to problem (4.13), the approximate equality constrained problem is obtained

$$\begin{aligned} & \min_{(\mathbf{y},\mathbf{s})} f_\sigma(\mathbf{y},\mathbf{s}) = \min_{(\mathbf{y},\mathbf{s})} \left(f(\mathbf{y}) - \sigma \sum_i \ln(s_i) \right) \\ \text{subject to} \quad & g(\mathbf{y}) + \mathbf{s} = \mathbf{0} \\ & \mathbf{h}(\mathbf{y}) = \mathbf{0} \\ & \mathbf{s} \geq \mathbf{0} \ , \end{aligned} \tag{4.22}$$

where $\sigma > 0$ is the barrier parameter.

The corresponding Lagrangian is

$$\mathcal{L}(\mathbf{y},\mathbf{s},\boldsymbol{\mu},\boldsymbol{\lambda}) = f(\mathbf{y}) - \sigma \sum_{i=1}^{m} \mu_i \ln(s_i) + \sum_{i=1}^{m} \mu_i \left(g_i(\mathbf{y}) + s_i \right) + \sum_{j=1}^{t} \lambda_j h_j(\mathbf{y})$$

If possible, the approximate problem (4.22) is solved at each iteration by a direct step, which is explained below.

Direct step During a direct step, the corresponding KKT-equations

$$\begin{aligned} \nabla_{\mathbf{y}}\mathcal{L}(\mathbf{y},\mathbf{s},\boldsymbol{\mu},\boldsymbol{\lambda}) = \nabla f(\mathbf{y}) + \sum_{i=1}^{m}\mu_i\nabla g_i(\mathbf{y}) + \sum_{j=1}^{t}\lambda_j\nabla h_j(\mathbf{y}) &= \mathbf{0} \\ \nabla_{\mathbf{s}}\mathcal{L}(\mathbf{y},\mathbf{s},\boldsymbol{\mu},\boldsymbol{\lambda}) = -\sigma\sum_{i=1}^{m}\frac{1}{s_i} + \sum_{i=1}^{m}\mu_i &= 0 \\ \mathbf{h}(\mathbf{y}) &= \mathbf{0} \\ \mathbf{g}(\mathbf{y}) + \mathbf{s} &= \mathbf{0} \end{aligned} \tag{4.23}$$

are solved through linear approximation by Newton's method. The resulting linear equation is solved by an LDL factorization. This factorization is the most computationally expensive step. During this step is determined whether the projected Hessian is positive definite and therefore the approximate problem is locally convex near the current iterate. If this does not apply, the algorithm takes a conjugate gradient step instead of this direct step.

Conjugate gradient step The conjugate gradient approach minimizes a quadratic approximation to the approximate problem within a trust region.

Generally, for a trust region method an approximate function is minimized. This function has to be close to the objective function for all points within a certain radius R around the current point x_k. The search of a minimum $x_k + \Delta x_k$ is restricted to points within this region, so $\Delta x_k \leq R$ is postulated.

Fist the Lagrange multipliers are calculated by approximately solving the KKT equations (4.23) in the sense of least-squares, whereas $\boldsymbol{\mu}$ is kept positive. Following notations are used

- $\mathbf{J_g}$ denotes the Jacobian of the inequality constraint function $\mathbf{g}$
- $\mathbf{J_h}$ denotes the Jacobian of the equality constraint function $\mathbf{h}$

- $\mathbf{S} = \mathrm{diag}(\mathbf{s})$
- $\boldsymbol{\mu}$ denotes the Lagrange multiplier vector associated with constraints $\mathbf{g}$
- $\mathbf{M} = \mathrm{diag}(\boldsymbol{\mu})$
- $\mathbf{e}$ denotes the vector of ones the same size as $\mathbf{g}$

In order to obtain new solution $(\mathbf{y} + \Delta\mathbf{y}, \mathbf{s} + \Delta\mathbf{s})$

$$\min_{\Delta\mathbf{y},\Delta\mathbf{s}} \nabla f^T \Delta\mathbf{y} + \frac{1}{2}\Delta\mathbf{y}^T \nabla^2_{\mathbf{yy}} \mathcal{L} \Delta\mathbf{y} + \boldsymbol{\mu}\mathbf{e}^T \mathbf{S}^{-1} \Delta\mathbf{s} + \frac{1}{2}\Delta\mathbf{s}^T \mathbf{S}^{-1}\mathbf{M}\Delta\mathbf{s}$$

is approximately solved. Following linearized constraints hold

$$\mathbf{g}(\mathbf{y}) + \mathbf{J}_\mathbf{g}\Delta\mathbf{y} + \Delta\mathbf{s} = \mathbf{0}\,, \quad \mathbf{h}(\mathbf{y}) + \mathbf{J}_\mathbf{h}\Delta\mathbf{y} = \mathbf{0}$$

and a norm of this constraints is minimized inside a trust region (radius R). Then the previous equation is solved, again the solution is to stay within the trust region and $\mathbf{s}$ is kept strictly positive.

The step size and direction are determined such that a merit function like

$$f_{\boldsymbol{\mu}}(\mathbf{y}, \mathbf{s}) + \nu \|(\mathbf{h}(\mathbf{y}), \mathbf{g}(\mathbf{y}) + \mathbf{s})\|$$

is decreased, where the parameter ν might be increased at each iteration.

Note For calculations in matlab, it is optional, whether bound constraints have to be satisfied during every step or whether they may be violated during intermediate iterations. In this work, the second option is chosen.

active-set algorithm

Many methods for solving for constrained minimization problems are based on solving the Karush-Kuhn-Tucker (KKT) equations

$$\begin{aligned} \nabla_x \mathcal{L}(x, \boldsymbol{\mu}, \boldsymbol{\lambda}) = \nabla f(x) + \sum_{i=1}^{m} \mu_i \nabla g_i(x) + \sum_{j=1}^{t} \lambda_j \nabla h_j(x) &= \mathbf{0} \\ \mathbf{g}(x) &\leq \mathbf{0} \\ \mathbf{h}(x) &= \mathbf{0} \\ \boldsymbol{\mu} &\geq \mathbf{0} \\ \boldsymbol{\mu}^T \mathbf{g}(x) &= \mathbf{0} \ . \end{aligned}$$

The last two conditions imply that only Lagrange multipliers of active constraints have to be determined, for inactive ones the Lagrange multipliers are zero.

Solving the KKT equations is basis of many nonlinear programming algorithms where Lagrange multipliers are directly computed. Here a constrained quasi-Newton method is applied, which provides for superlinear convergence. It is also known as Sequential Quadratic Programming (SQP) method since a Quadratic Programming (QP) subproblem is solved at each major iteration. QP is also called iterative Quadratic Programming, Recursive Quadratic Programming or Constrained variable metric method.

Sequential Quadratic Programming (SQP) This method approximates the Lagrangian function (4.16) of problem (4.13) at each iteration by a quadratic subproblem. The Hessian of the Lagrangian is denoted by $\mathbf{H}$,

$$\mathbf{H}(x, \boldsymbol{\mu}, \boldsymbol{\lambda}) = \nabla_{xx} \mathcal{L}(x, \boldsymbol{\mu}, \boldsymbol{\lambda}) = \nabla_{xx} f(x) + \sum_{i=1}^{m} \mu_i \nabla_{xx} g_i(x) + \sum_{j=1}^{t} \lambda_j \nabla_{xx} h_j(x) \ .$$

For calculations in Matlab, at each step the Hessian is approximated numerically by using quasi-Newton updating method. It is kept positive definite at each step.

The nonlinear constraints are linearized, and then the quadratic programming subproblem is given by

$$\begin{aligned} & \min_d \frac{1}{2}\mathbf{d}^T\mathbf{H}(x_k,\boldsymbol{\mu},\boldsymbol{\lambda})\mathbf{d} + \nabla f(x_k)^T\mathbf{d} \\ \text{subject to} \quad & \nabla g_i(x_k)^T d + g_i(x_k) \leq 0, \quad i = 1...m \\ & \nabla h_i(x_k)^T d + h_i(x_k) = 0, \quad i = 1...t \quad . \end{aligned}$$

This problem is solved by using an active set strategy, which is also known as projection method. The new iterate is

$$x_{k+1} = x_k + \alpha_k d_k \quad ,$$

where the step length α is obtained by doing a line search such that a merit function is decreased sufficiently. The used merit function is given as

$$\Psi(x) = f(x) + \sum_{j=1}^{t} r_j^h h_j(x) + \sum_{i=1}^{m} r_i^g \max[0, g_i(x)] \quad ,$$

and the penalty parameters are

$$\begin{aligned} r_i^g = (r_{k+1}^g)_i &= \max_i \left\{ \mu_i, \tfrac{(r_k^g)_i + \mu_i}{2} \right\}, \qquad i = 1...m \\ r_i^h = (r_{k+1}^h)_i &= \max_j \left\{ \lambda_i, \tfrac{(r_k^h)_i + \lambda_i}{2} \right\}, \qquad i = 1...t \quad . \end{aligned}$$

The initial values for r_i^g and r_i^h are set to

$$\begin{aligned} r_i^g &= \tfrac{\|\nabla f(x)\|}{\|\nabla g_i(x)\|}, \qquad i = 1...m \\ r_i^h &= \tfrac{\|\nabla f(x)\|}{\|\nabla h_i(x)\|}, \qquad i = 1...t \quad . \end{aligned}$$

SQP methods are state of the art in nonlinear programming. They solve some nonlinear constrained problems faster than unconstrained problems as e.g. the feasible area is limited and therefore there exists more information regarding the search direction and step length.

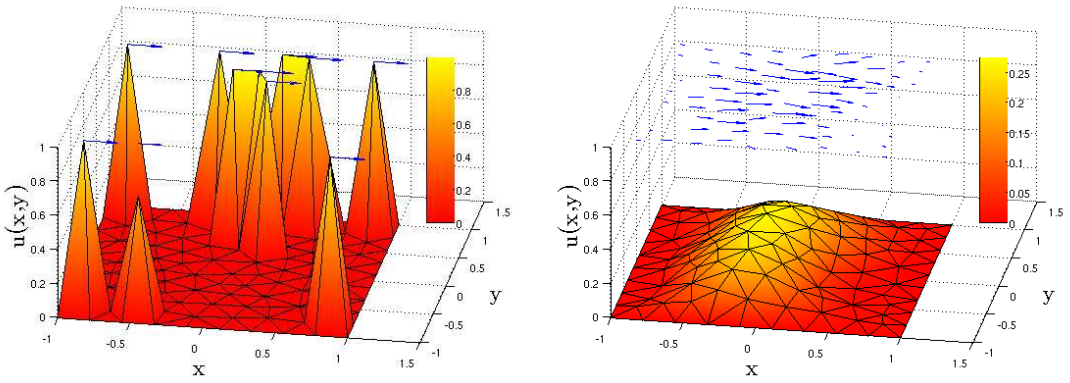

Figure 4.2: Example of simulation results

4.3.3 Software

All calculations are done with Matlab version 7.8.0 (R2009a). For optimization the Matlab solver *fmincon* is used, which is included in the optimization toolbox. This solver provides for the use of interior point algorithm as well as active-set algorithm. In practice the interior point algorithm is significant faster. Some calculations were done by both algorithms and no difference in the resulting u and $\mathbf{m}$ were evident.

The mesh is generated by the freeware generator gmsh [28]. The finite element discretization is based on the Matlab FEM program *50 lines of Matlab* by C. Carstensen, which is explained in [32]. The elementwise matrices are justified by calculations with Maple version 10.06 .

4.4 Results of simulation

In this section the results of the simulation are shown. Especially the influence of the different parameters is illustrated. Figure 4.2 shows typical results. It displays the distribution function u over the domain $\Omega = [-1, 1] \times [-1, 1]$, where the unit is mm. The colorbar on the right hand side of a figure assigns colors to the different values of u. It is interpolated between the

maximal and the minimal value that occur in one figure. Thus the colorbar ranges from 0 to 1 on the figure to the left and from 0 to 0.3 on the figure to the right. The blue arrows illustrate the direction and the effective strength of the magnetization $\mathbf{m}$, which is obtained from the simulation result multiplied by u.

The mesh consists of 190 triangular elements over Ω for simulation of u and $\mathbf{m}$ and of 2114 additional over Ω_V for simulation of the potential V. The number of nodes is 114 respectively 1069.

Following table gives an overview over the investigated range of parameter values as well as the optimal set of parameters:

name	$\frac{\varepsilon_2^2}{2}$	$\frac{\varepsilon_4^2}{4}$	α	A	M_S	$\mathbf{H_{ext}}$
range	$10^{-12} - 10^{8}$	$10^{-12} - 10^{8}$	$10^{-15} - 10^{15}$	$10^{-1} - 10^{10}$	$10^{0} - 10^{7}$	$10^{-1} - 10^{10}$
optimal	0.1	0.01	10^{5}	10^{-8}	10^{7}	10^{4}

The left picture of figure 4.2 results if these parameters are used and the external field is applied in x direction. If not otherwise specified, these values, an external field in x direction, and a particle concentration of 8 % are used for simulation.

4.4.1 Convergence

Minimizing the functional (4.1) according to u and $\mathbf{m}$ successively instead of simultaneously leads definitely to faster convergence as then the number of minimizing variables in one run is significant lower. The results are similar, therefore the simulation is done by a successive process over which is iterated. For most parameter sets the results of 3 and 5 iterations do not differ, particularly not for the optimal parameter set.

A minimizing process should stop at a feasible local minimum. Because of computational inaccuracy the numerical algorithm stops if one of the following criteria that indicate a local

minimum is met: The change in the variable is less than tolerance T_1. For constrained optimization the constraint violation has to be less than tolerance T_2. For equality constraints $\mathbf{h}(\mathbf{y}) = 0$ that means that $\tilde{\mathbf{y}}$ is optimal if $|\mathbf{h}(\tilde{\mathbf{y}})| < T_2$. The first-order optimality measure has to be less than tolerance T_3. This criterion is consistent with $f'(x) = 0$ in the unconstrained one-dimensional case. These criteria are met for most parameter sets.

In order to prevent infinite loops, the algorithm stops also if more than T_4 function evaluations are done. This happens sometimes during the first iteration, seldom also during the second or later. An increase of T_4 does not provide significant better results. The algorithm stops also if T_1 is met but not T_2 as then no adjacent feasible point is found.

Thus not for every parameter set an optimal point where all convergence criteria are met is found. A further investigation of the convergence criteria remains for future work.

A reduction of the functional value seems also to be a suitable indicator of minimization. But the algorithm allows for provisional results that are not feasible. The algorithm does not stop at such a point as then tolerance T_2 is hurt but the function value might be lower at such a point.

The simulation accomplished with the optimal parameter set converges by means of this criteria on the standard mesh. If the optimal parameter set is used for simulation on a refined mesh, convergence is not achieved, even though the tolerance criteria are modified slightly. This is subject to further research.

4.4.2 Initial values

Even though a stationary model is considered, appropriate initial values are essential. Since the experiments are started by dropping some ferrofluid on a surface, it is assumed that the particles are gathered in the middle of the domain Ω. The magnetic moments are expected to align according to the external field. Therefore, this direction is chosen at the beginning. The

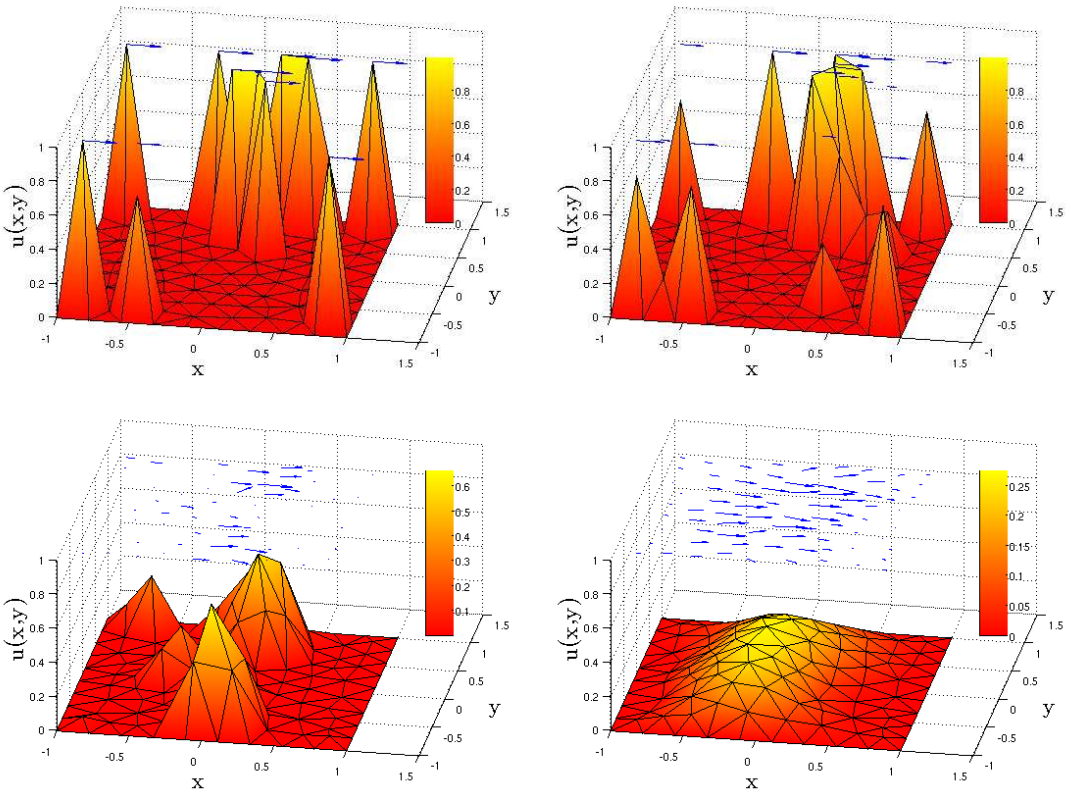

Figure 4.3: Influence of the interaction lengths ε_4 and ε_2.

simulation results support these initial values. A variation thereof remains for future work.

4.4.3 Parameters and their influence on the simulation

In order to examine the influence of the different parameters on the total energy (4.1) and to obtain the best result, different values for these parameters are tested. The domain is measured in mm, therefore the parameters are given in SI units and in units of mm.

Interaction lengths ε_4 and ε_2

According to Cahn and Hilliard, cf. [4, 5], the interaction lengths ε_4 and ε_2 are small compared to characteristic dimensions on the laboratory scale. They are multipliers to the gradients and appear in the energy functional (4.1) in the terms $\frac{\varepsilon_4^2}{4}|\nabla u|^4$ and $\frac{\varepsilon_2^2}{2}|\nabla u|^2$. Thus they control the influence of the gradient on the energy. Larger values of ε_4 and ε_2 provide for a smoother distribution u since then any change in u is penalized which leads to a larger overall energy.
It is investigated

- change of ε_2
- change of ε_4
- simultaneous change of both parameters.

By employing values between 10^{-12} and 10^2 for $\frac{\varepsilon_2^2}{2}$, $\frac{\varepsilon_4^2}{4}$ or both of them, no influence on the distribution function is detected, see top left in figure 4.3. If the value is increased further, the distribution function flattens as expected, compare figure 4.3, where the result is shown for the values 10^3 (top right), 10^5 and 10^7. A value of 10^7 leads to a smooth distribution u with a maximal value of 0.3. The figures show the results for a simultaneous change of both parameters, the change of just one parameter leads to similar results.
The values assigned for further simulation are $\frac{\varepsilon_4^2}{4} = 0.01$ and $\frac{\varepsilon_2^2}{2} = 0.1$. These values are smaller than the diameter of Ω, which is a characteristic dimension in this problem. It is given by 2. The size of a particle, which is assumed to be $1.2{\cdot}10^{-5}$ mm, is another characteristic length of this problem. As stated above, a choice of the interaction lengths in this dimension would lead to the same simulation results.

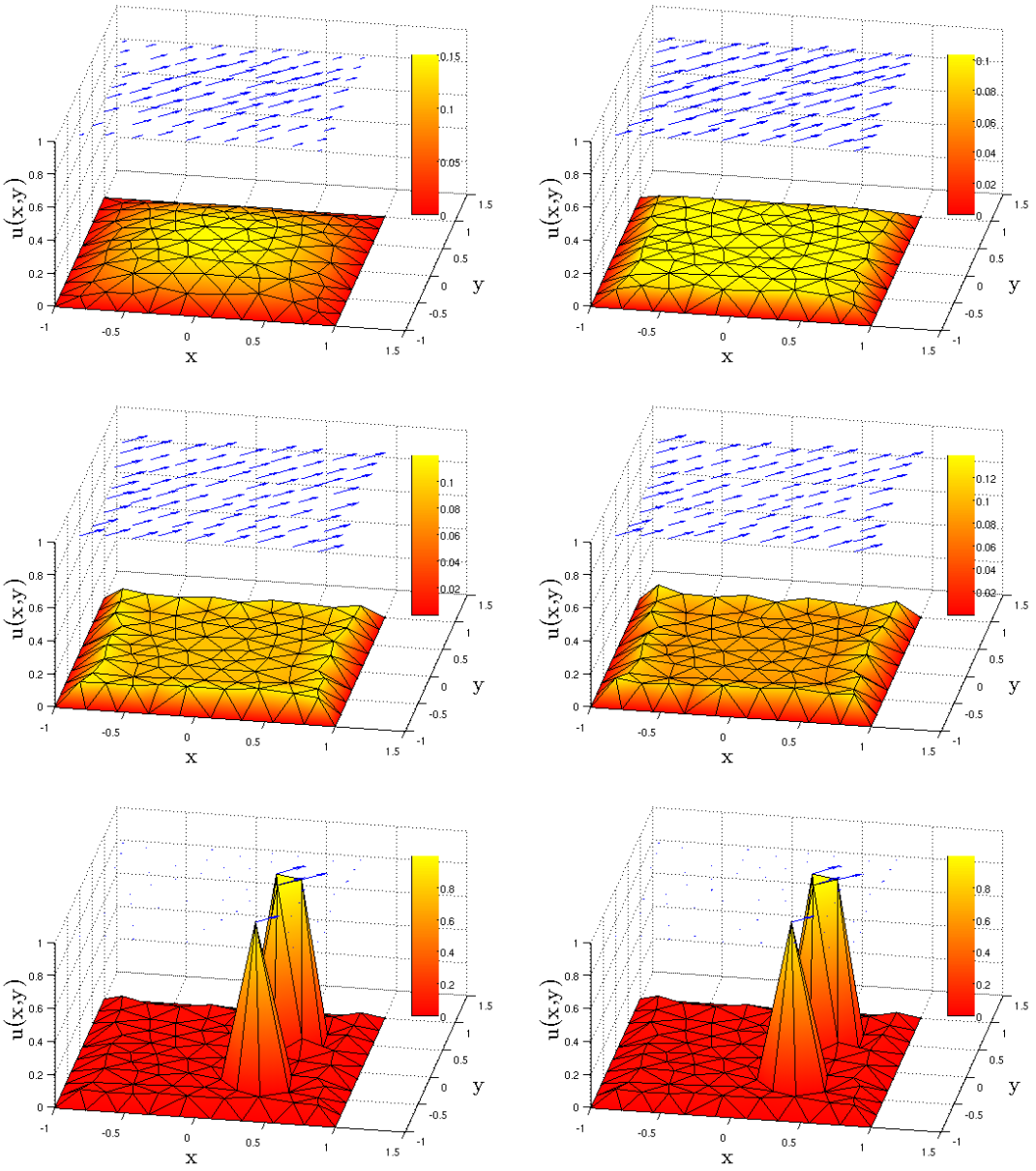

Figure 4.4: Influence of multiplier α if the remaining parameters are equal one.

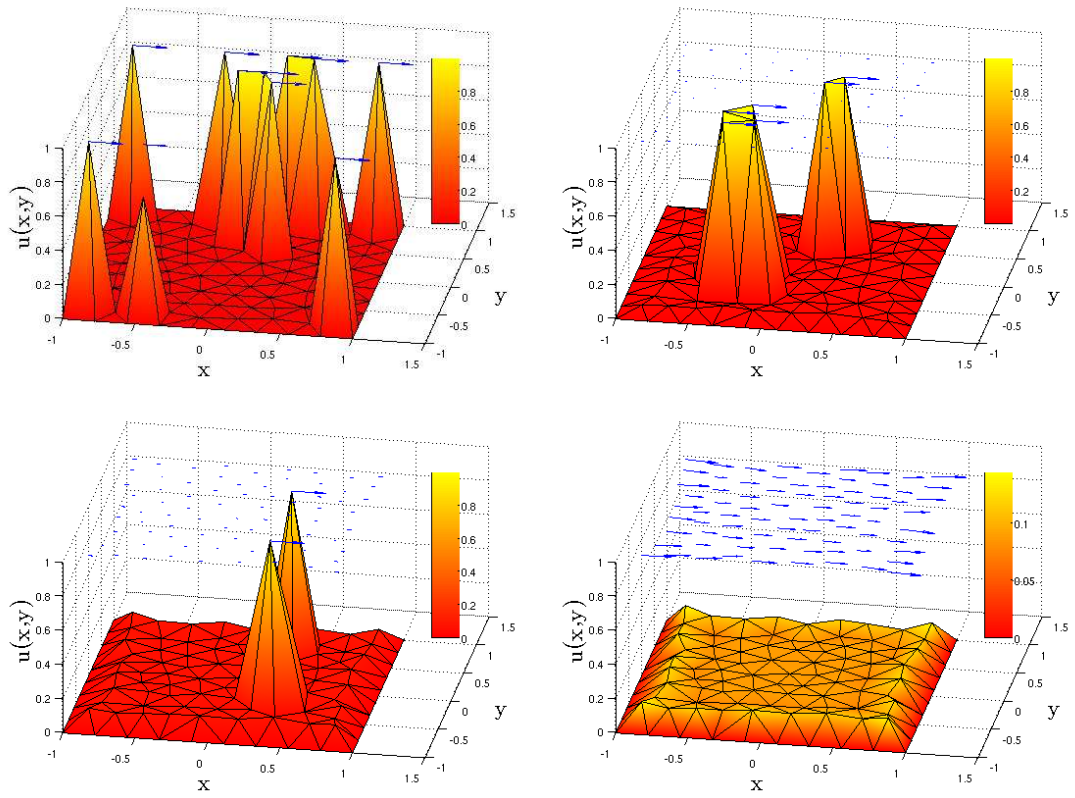

Figure 4.5: Influence of multiplier α if standard values are assigned to the remaining parameters.

Multiplier α

The multiplier α controls the influence of the considered free energy density $W(u) = \alpha u^2(1-u)^2$ on the total energy. Because of this definition of $W(u)$, it is expected that a large value provides for u to be likely 0 or 1 and a low value leads to an even distribution. This influence is in evidence if the remaining parameters are set equal one and only the particle concentration is 8%, see figure 4.4. The values of α are increased by a factor of ten from 10 at top left to 10^6 bottom right. A further increase of α up to 10^{12} does not change the result.

If optimal values are assigned to the remaining parameters, a variation of α from 10^{-15} to 10^6 does not influence the resulting u and $\mathbf{m}$. Raising α above 10^6 changes the pattern of u: the sides arch upwards and the distribution is flattened, compare figure 4.5. The values of α used for this figures are from top left 10^5, 10^{10}, 10^{12} and 10^{13}. This result is in contrast to the expected effect, which is received by setting the remaining parameters equal one, cf. figure 4.4. A sign flaw, which would be a reasonable explanation, is excluded but the cause of this result is not identified yet.

For simulation the value $\alpha = 10^5$ is assigned.

Exchange stiffness constant A

The exchange stiffness constant A is a weakly temperature dependent material constant. As this thesis considers a constant temperature, also a constant value of A is used. For ferromagnetica it is within the range of $10^{-12} - 2 \cdot 10^{-11}$ J/m, cf. [14], which equals $10^{-9} - 2 \cdot 10^{-8}$ kg mm/s^2. The stiffness constant is necessary to calculate the exchange energy density $A\,|\boldsymbol{\nabla}\mathbf{m}|^2\,u$ which penalizes deviations from a homogeneous magnetization. Since the magnetization is already nearly homogeneous and thus the gradient is everywhere on Ω close to zero, the influence of a change in A on the result is estimated to be very small. Indeed, for $10^{-15} \leq A \leq 10^{-1}$ no

change in the result was detected.

For simulation $A = 10^{-8}$ is assigned which is within the admissible range.

Saturation magnetization M_S

The saturation magnetization M_S is the maximal magnetic moment that can be obtained in an applied external magnetic field. It depends on the material, the size of the particle and the size of the particle shell. A ferromagnetic particle with a diameter of 12 nm has a saturation magnetization of approximately 600 to 1800 A/mm, cf. Section 2.2.1.

M_S is needed for the calculation of two terms of the energy functional (4.1): for the Zeeman energy density $-\mu_0 M_S \mathbf{H_{ext}} \cdot \mathbf{m} \cdot u$ and for the stray field energy density $0.5\mu_0 M_S \nabla V \cdot \mathbf{m} \cdot u$. Further it is used to define the scalar potential V, which belongs to the stray field $\mathbf{H_d}$, as V is calculated by means of $\Delta V = M_S \mathrm{div}\,(\chi_\Omega \mathbf{m})$. Thus its influence on the stray field energy density is indeed quadratic. Therefore a strong influence on the particle distribution u and the magnetization $\mathbf{m}$ is expected if M_S is changed.

This influence is displayed in figures 4.6 and 4.7, where the value of M_S is increased from 10^{-1} top left to 10^4 bottom right and from 10^5 top left to 10^{10} bottom right. The result for an applied external field in y direction confirms that the optimal value is 10^7, which is larger than expected. As M_S should even decrease with decreasing particle diameter, this effect is not explained yet.

External field $\mathbf{H_{ext}}$

The experimental results suggest that the direction the strength of the external field has a strong influence on the particle distribution. Fields of 0.1 to 1 T were used for the experiments. The strength of the external field determines the influence of the Zeeman energy density $-\mu_0 M_S \mathbf{H_{ext}} \cdot \mathbf{m} \cdot u$.

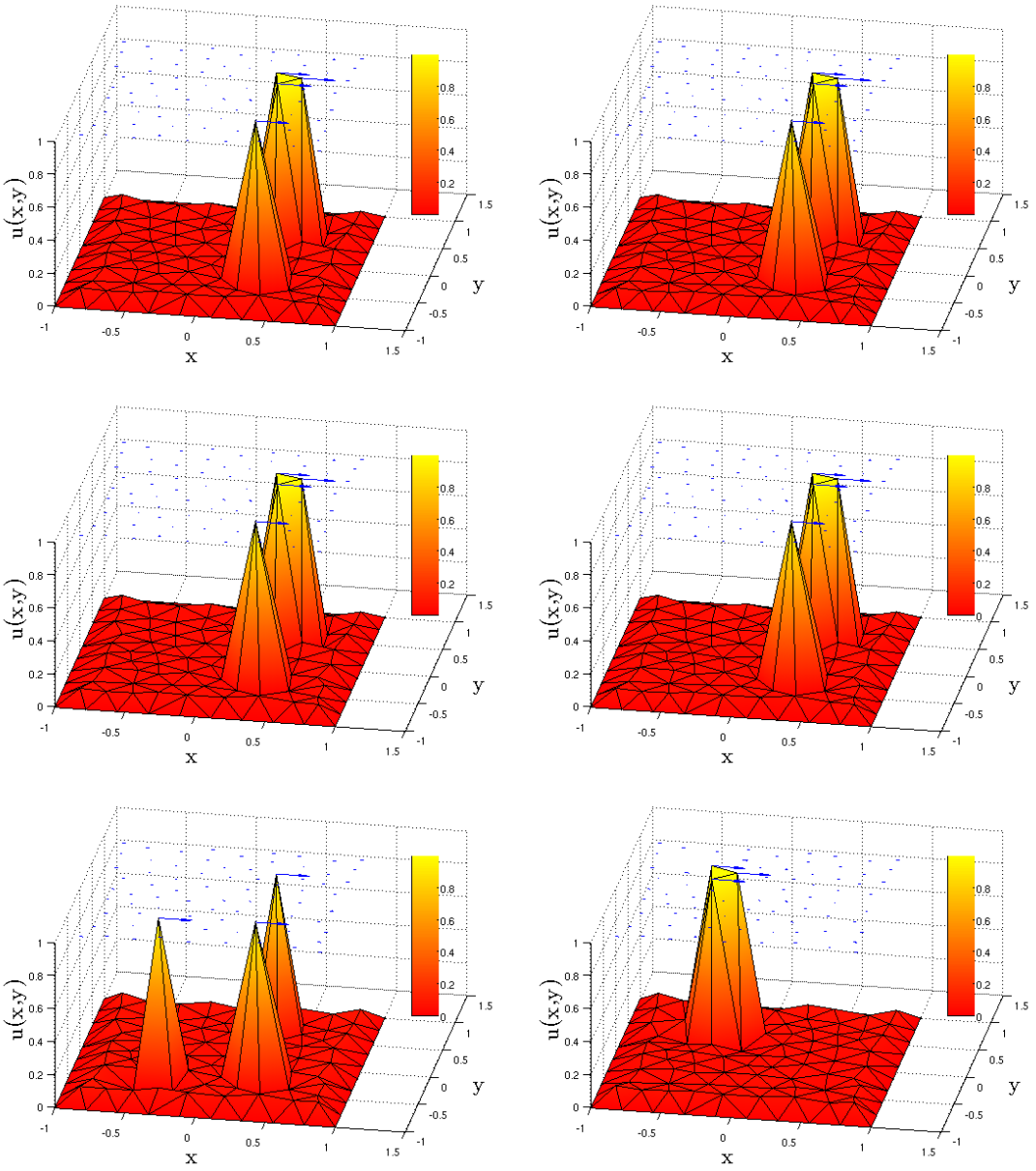

Figure 4.6: Influence of the saturation magnetization M_S on the particle distribution.

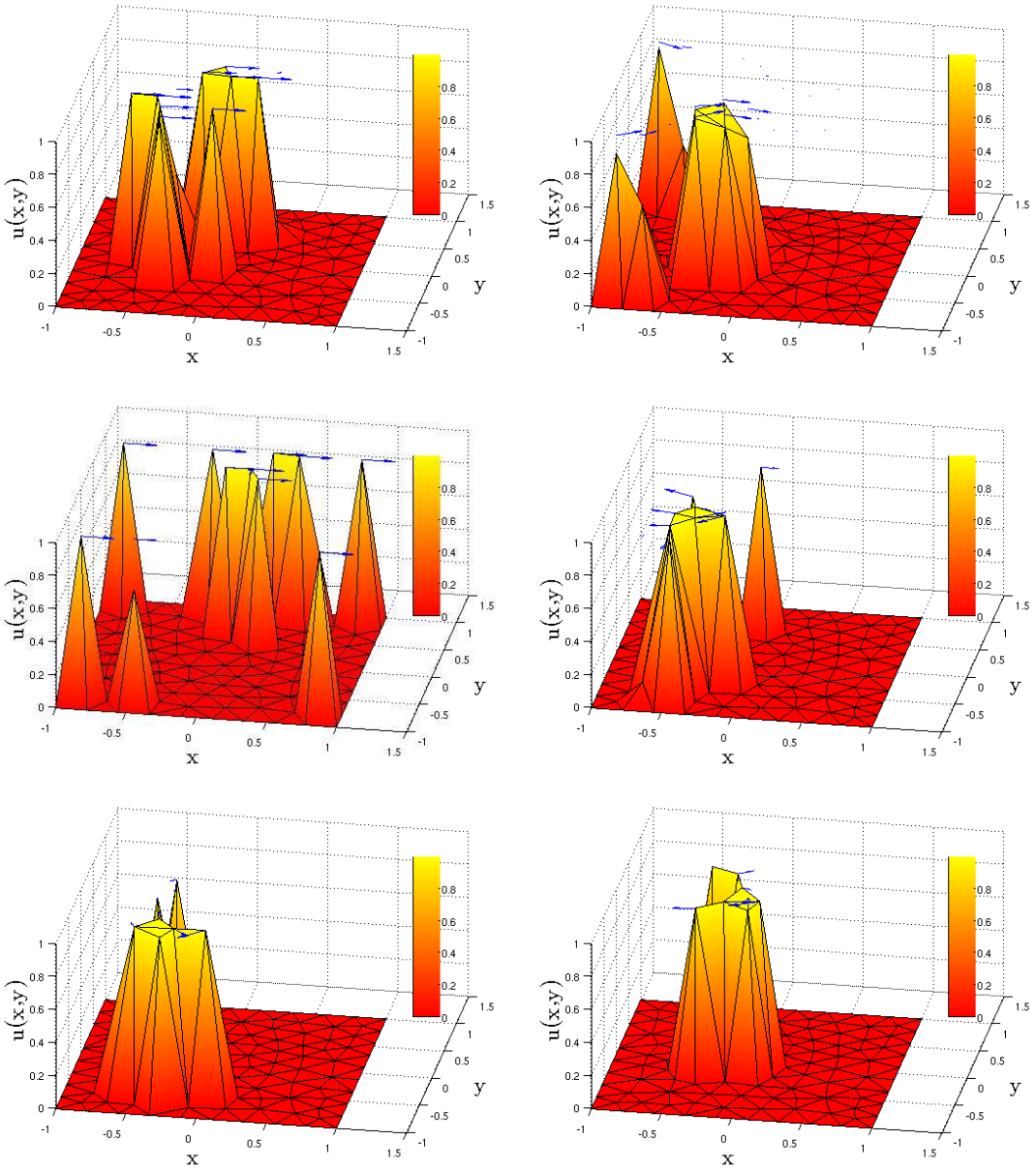

Figure 4.7: Influence of the saturation magnetization M_S on the particle distribution.

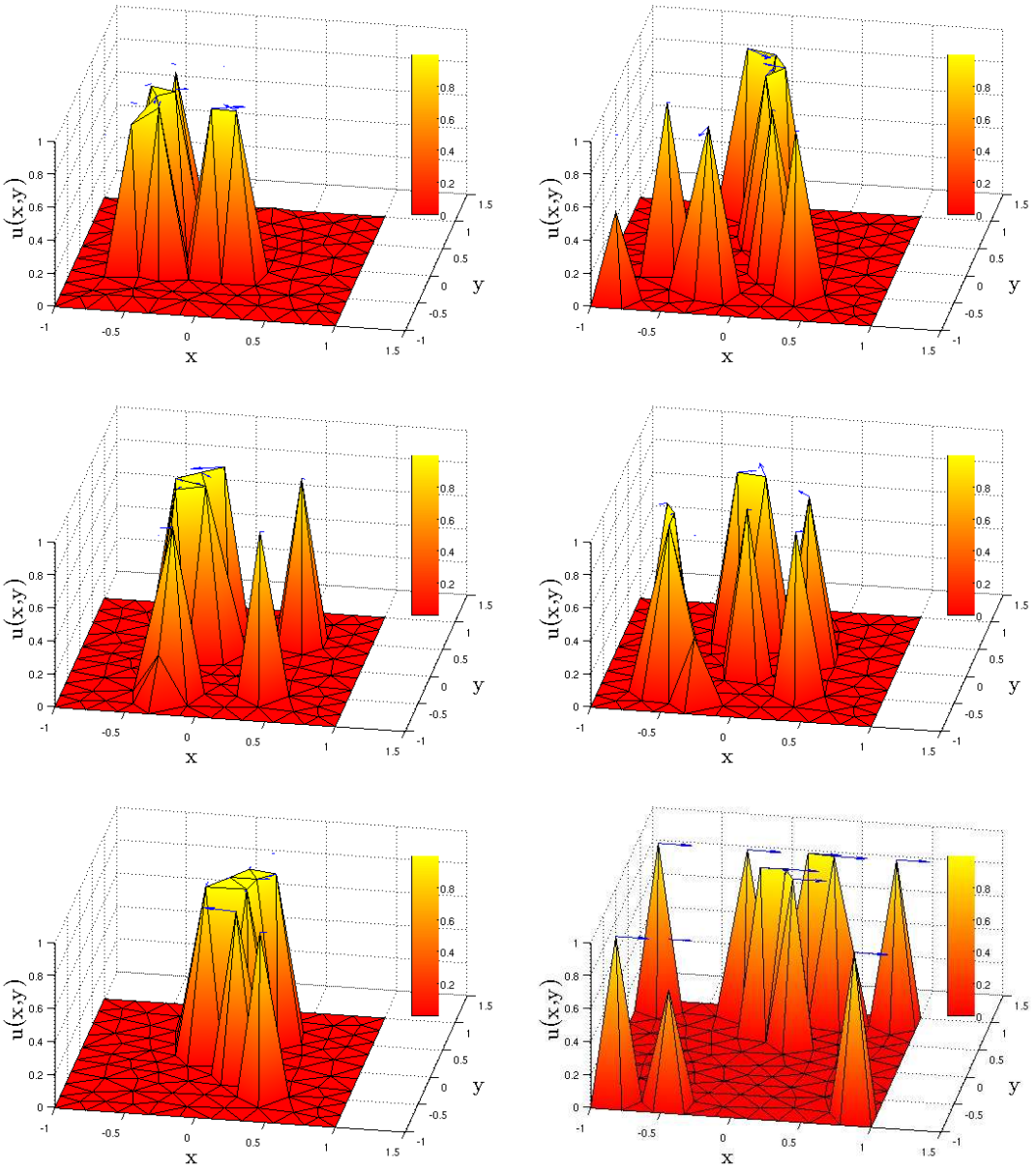

Figure 4.8: Influence of an external field $\mathbf{H_{ext}}$ in x direction on the particle distribution.

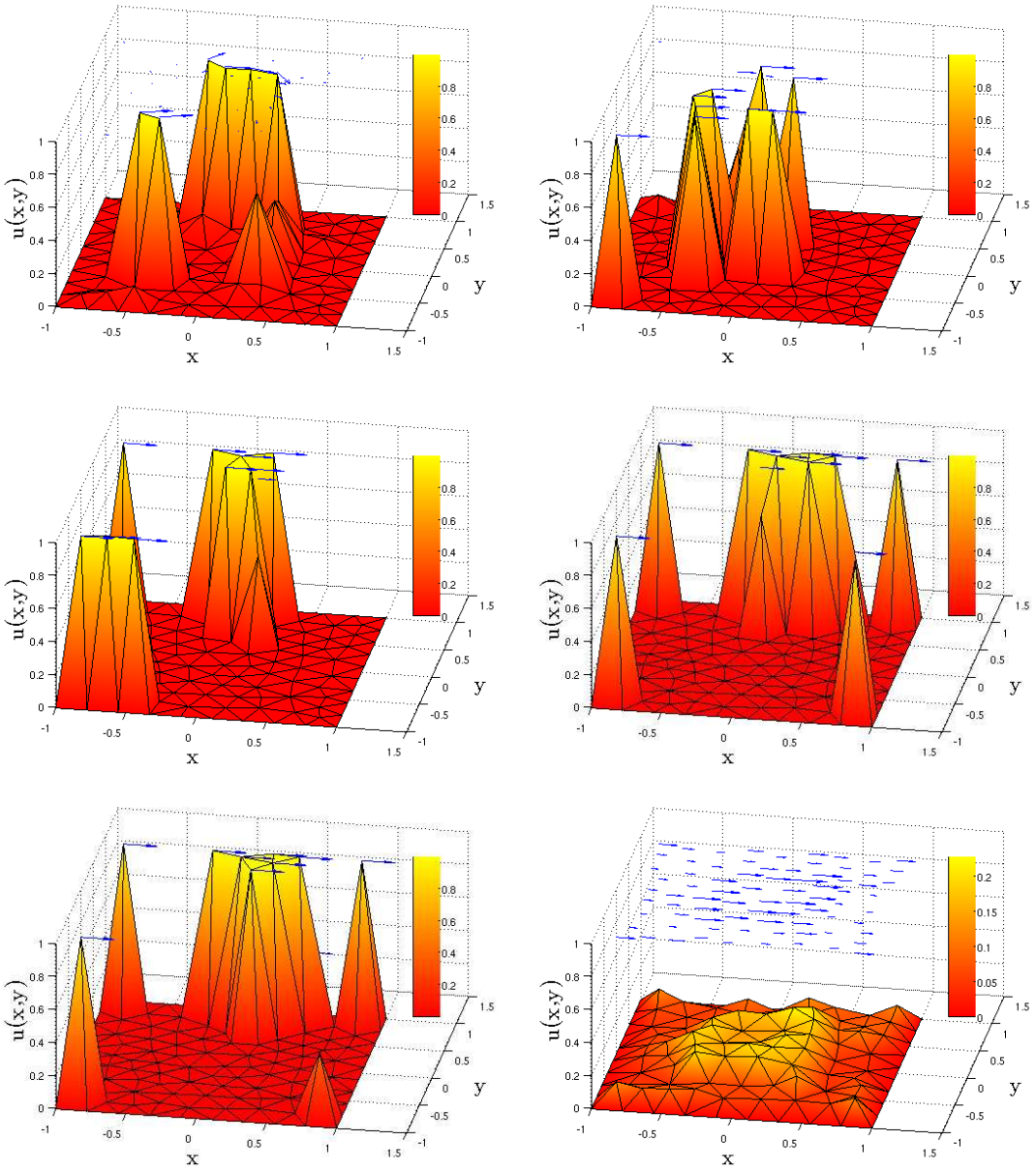

Figure 4.9: Influence of an external field $\mathbf{H_{ext}}$ in x direction on the particle distribution.

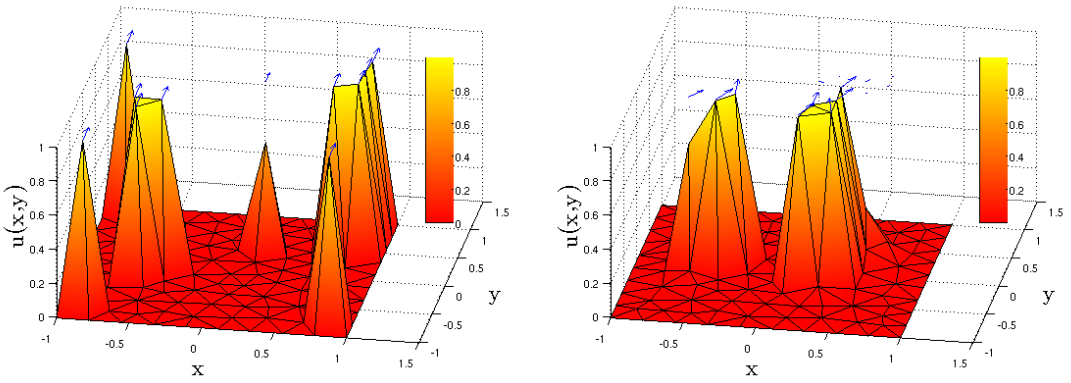

Figure 4.10: Influence of an external field $\mathbf{H_{ext}}$ in y direction on the particle distribution.

An influence of the external field on the particle distribution is evident, compare figures 4.8 and 4.9, where the external field in x direction is increased by a factor of ten from 10^{-1} to 10^{10} T. As expected, the particles form broader clusters under an enhanced field, which is clearly visible for a field in x direction if e.g. the picture bottom right of figure 4.8 is compared to the picture bottom left of figure 4.9. The alignment of the particle clusters according to the external field starts at a strength of 10^4, which is higher than expected. A lower field does not suffice to align the magnetic moments, either. The last picture of figure 4.9 shows a flat and smooth distribution: the particles form one cluster under the influence of a very strong field.

Also for a field in y direction the formation of clusters according to the field direction and strength is evident, compare figure 4.10 for $\mathbf{H_{ext}} = 10^4$ and $\mathbf{H_{ext}} = 10^5$.

The same good result as for $\mathbf{H_{ext}} = 10^4$ and $M_S = 10^7$ is also achieved for $\mathbf{H_{ext}} = 10^5$ and $M_S = 10^8$ or $\mathbf{H_{ext}} = 10^6$ and $M_S = 10^9$ but not for lower values of these two parameters. This indicates a strong influence of the Zeeman energy as both parameters are needed for the calculation thereof.

Vacuum permeability μ_0

The vacuum permeability is a physical constant that is defined as

$$\mu_0 = 4 \cdot \pi \cdot 10^{-7} \frac{\mathrm{Vs}}{\mathrm{Am}} = 4 \cdot \pi \cdot 10^{-4} \frac{\mathrm{kg\ mm}}{\mathrm{A^2 s^2}} \quad .$$

It influences the Zeeman energy density and the stray field energy density.

Since μ_0 is a physical constant, a variation thereof is not investigated.

Particle concentration

Since the amount of particles is conserved during one simulation, the equality constraint $\int_\Omega u \, d\mathbf{x} = c \cdot |\Omega|$ holds, where $|\Omega|$ denotes the area of Ω. So the particle concentration c defines the percentage of the domain Ω that is covered by particles. It is changed in order to confirm the optimal parameter set. The cluster size should be increased by a higher particle concentration but the clusters should always be aligned according to the external field.

The simulation results for different particle concentrations are displayed in figure 4.11 for 4 %, 6 %, 8 %, 13 %, 19 % and 24 %. There is no alignment observable for a particle concentration under 3 %, but for a higher concentration the alignment is always evident as expected.

4.4.4 Results

This chapter ends with the display of the optimal results for a field in x direction on the left and a field in y direction on the right of figure 4.12. The particles form clusters that are aligned to the applied external field.

One notices that the particle distribution is asymmetrically, e.g. for a field in positive x direction the particles tend to cluster closer to the border y = 1 than to y = −1. But this asymmetric effect does not go back to the influence of the external field as a field in negative x direction produces nearly the same distribution. Particularly, the particles are also then clustered closer

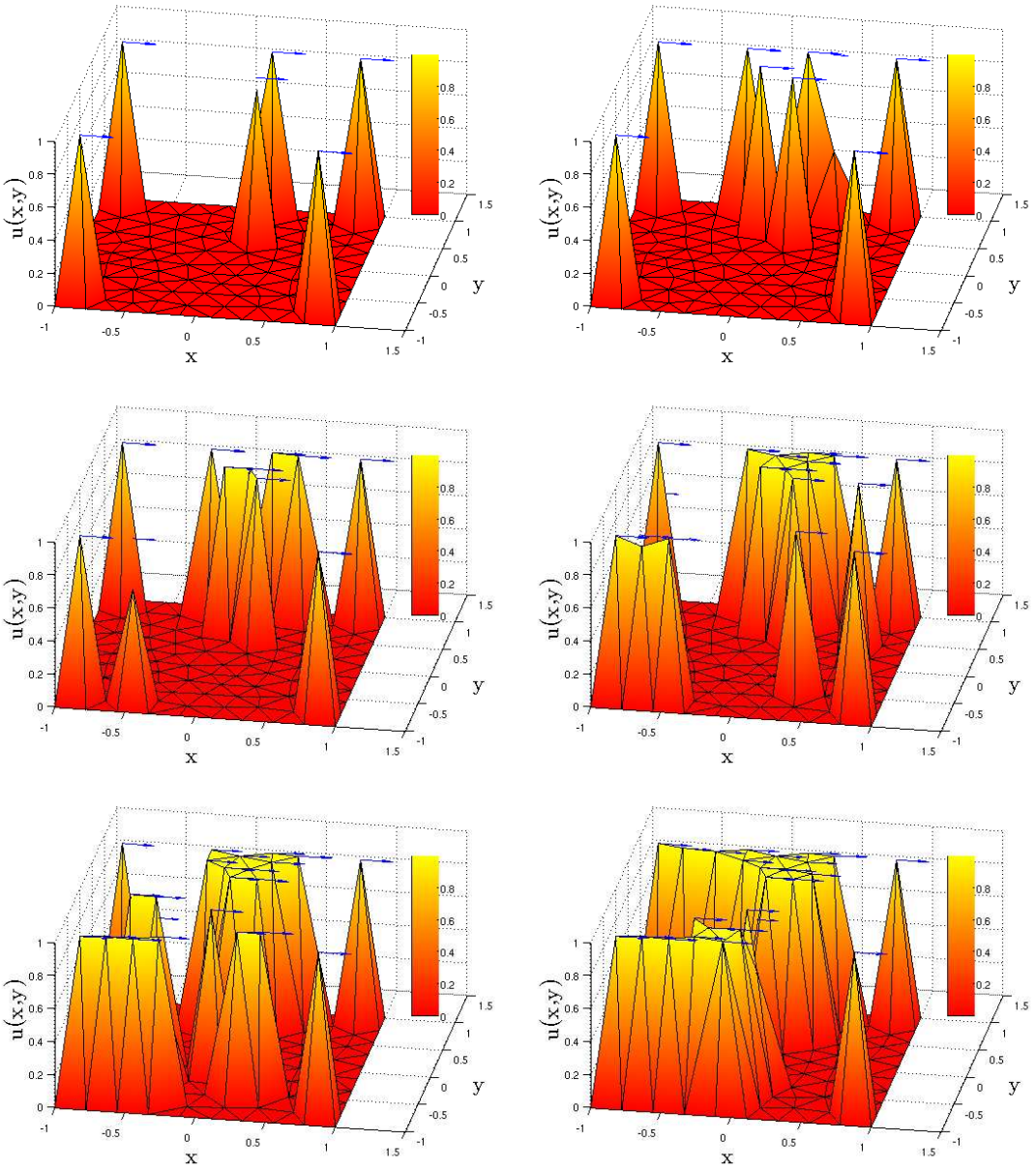

Figure 4.11: Different particle concentrations

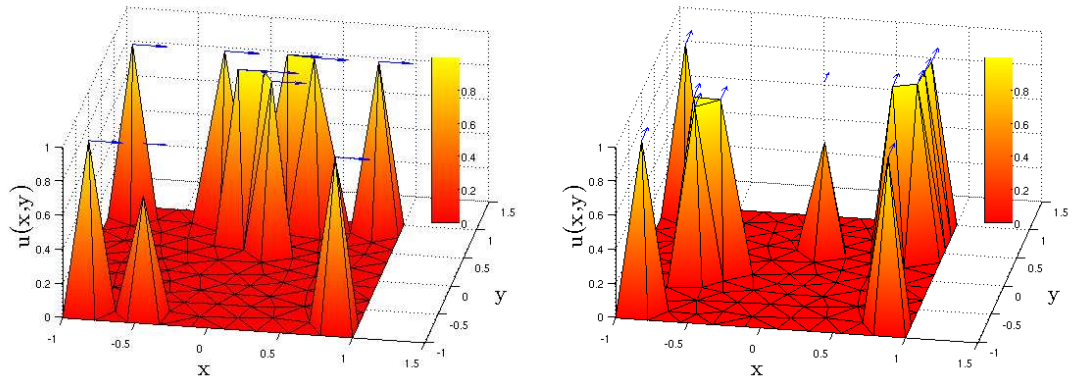

Figure 4.12: optimal results

to the border y = 1. Therefore, this asymmetric effect is rather up to numerical reasons. Moreover, the particles are gathered symmetrically in the middle of the domain Ω initially. Thus it is assumed that either the irregular mesh evokes this effect or that the algorithm prefers one search direction for minimization. This effect is under current investigation.

Chapter 5

Summary and perspective

In this thesis, a new two-dimensional model is derived that describes the pattern formed by a ferrofluid under the influence of an applied external magnetic field. The novelty of this model is the combination of the concept of micromagnetism with a particle distribution function. This function is controlled by the free energy model that Cahn and Hilliard [4, 5] proposed for a two component system. In this work, the two components are the particles and the fluid containing them. Moreover, the distribution function determines locally the intensity of the micromagnetic energy contribution. The micromagnetic energy depends also on the local magnetization. Since all particles are assumed to be magnetized to saturation, only a change in the direction of the local magnetization is studied. Thus the minimum of an energy model that depends on the distribution and the magnetization is determined. Mathematical analysis proves the existence of a solution to the model by the direct method. The simulation results reinforce the validity of the model as they are consistent with the theoretical predictions: they show a significant influence of the strength and direction of the external field on the particle distribution and the magnetic moment.

However, the parameter set for optimal results consists of values for the external field and the saturation magnetization that are significantly higher than physically reasonable. Thus the aim of future research is to achieve comparably good results using parameter values that are also experimentally observed. Since the mathematical model is a simplification of the distinct physical forces, a modification of the model should be taken into consideration. Moreover, changing the simulation process, the convergence criteria, or the initial values does not promise to solve this problem. Neglected forces that include a coupling of the saturation magnetization and the particle distribution may have the intended impact. Such a term might describe strong particle-particle interaction because of magnetic effects which are not covered by the Cahn-Hilliard model. Therefore such an additional term also makes sense physically. For the numerical part, this thesis concentrates on programming an appropriate algorithm and adapting the modeling parameters. Thus a modification of the energy functional has not been studied and is left for future work.

The parameters were not varied on a finer mesh because this would lead to substantially increasing computing time. First simulations on a finer mesh do not yet provide satisfying results. Another focal point for future research is the achievement of results on a finer mesh that are better than the results obtained in this thesis. Future work will also reconnect the simulation results with the application. Then the considered model could be adapted to similar experimental settings that meet practical or even industrial requirements and thus this work might be carried from fundamental research to real life application.

Appendix A

Analytical help

A.1 Boundedness of divergence of m

Be $\mathbf{m} \in W^{1,2}(\Omega, \mathbb{R}^2)$, where $\Omega \subset \mathbb{R}^2$, then $\boldsymbol{\nabla}\mathbf{m} : \mathbb{R}^2 \to \mathbb{R}^{2,2}$ and $\boldsymbol{\nabla}\mathbf{m} \in L^2(\Omega)$ and thus

$$\|\boldsymbol{\nabla}\mathbf{m}\|^2_{L^2(\Omega)} = \int_\Omega \left(|\nabla m_1|^2 + |\nabla m_2|^2\right)\, d\mathbf{x} \tag{A.1}$$

$$= \int_\Omega \left(m_{1,x}^2 + m_{2,x}^2 + m_{1,y}^2 + m_{2,y}^2\right)\, d\mathbf{x} < \infty \tag{A.2}$$

Since the gradient $\boldsymbol{\nabla}\mathbf{m}$ is isomorphic to a function $\mathbb{R}^2 \to \mathbb{R}^4$, it is w.l.o.g. considered as such in the following.

Proposition A.1. *If* $\mathbf{m} \in W^{1,2}(\Omega, \mathbb{R}^2)$*, then* $div\mathbf{m} \in L^2(\Omega)$.

Proof.

$$\begin{aligned}
\|\operatorname{div}\mathbf{m}\|^2_{L^2(\Omega)} &= \int_\Omega \left(|m_{1,x}+m_{2,y}|^2\right)\, d\mathbf{x} && \text{(A.3)}\\
&= \int_\Omega \left(m^2_{1,x}+2|m_{1,x}|\,|m_{2,y}|+m^2_{2,y}\right)\, d\mathbf{x} && \text{(A.4)}\\
&\le \int_\Omega 2\left(m^2_{1,x}+m^2_{2,y}\right)\, d\mathbf{x} && \text{(A.5)}\\
&\le 2\int_\Omega \left(m^2_{1,x}+m^2_{2,x}+m^2_{1,y}+m^2_{2,y}\right)\, d\mathbf{x} && \text{(A.6)}\\
&= 2\|\boldsymbol{\nabla}\mathbf{m}\|^2_{L^2(\Omega)} < \infty && \text{(A.7)}
\end{aligned}$$

Furthermore, if $\mathbf{m}$ is expanded to the whole space $\mathbb{R}^2$, where $\mathbf{m}\equiv 0$ on $\mathbb{R}^2\setminus\Omega$, then obviously the above holds also on $\mathbb{R}^2$. □

Appendix B

Discretization

This appendix chapter refers to Section 4.2.2. Here the discretization of the considered energy functional

$$\begin{aligned} E(u,\mathbf{m}) &= \int_\Omega \frac{\varepsilon_4^2}{4}|\nabla u|^4 + \frac{\varepsilon_2^2}{2}|\nabla u|^2 + W(u) \\ &\quad + \left(A\,|\boldsymbol{\nabla}\mathbf{m}|^2 - J_S\mathbf{H_{ext}}\cdot\mathbf{m} + \frac{1}{2}J_S\nabla V\cdot\mathbf{m}\right)\cdot u\; d\mathbf{x} \\ &= \int_\Omega \frac{\varepsilon_4^2}{4}|\nabla u|^4 + \frac{\varepsilon_2^2}{2}|\nabla u|^2 + W(u) + \varepsilon_{mag}^{loc}(\mathbf{m})\cdot u\; d\mathbf{x} \\ &= \int_\Omega \varepsilon^{loc}(u,\mathbf{m})\; d\mathbf{x} \end{aligned} \tag{B.1}$$

is derived, where $\Omega \subset \mathbb{R}^2$.

B.1 Basis functions

The equation is discretized in the N-dimensional approximation space X_h, which is spanned on behalf of piecewise linear basis function η_j, $j = 1...N$, which have a compact support and $\eta_i(\mathbf{x}_j) = \delta_{ij}$ for $i, j = 1...N$. The distribution function u and the magnetization vector $\mathbf{m}$ are

approximated in X_h by a linear combination of the basis functions such that

$$u_h(\mathbf{x}) = \sum_{j=1}^{N} u_j \cdot \eta_j(\mathbf{x}) \qquad \text{and} \qquad \mathbf{m}_h(\mathbf{x}) = \sum_{j=1}^{N} \mathbf{m}_j \cdot \eta_j(\mathbf{x}) = \sum_{j=1}^{N} \begin{pmatrix} m_{j,1} \\ \\ m_{j,2} \end{pmatrix} \cdot \eta_j(\mathbf{x}) \quad . \tag{B.2}$$

Thus the coefficient vectors are defined as $\mathcal{U} := (u_1, ..., u_N)^T$, $\mathcal{M}_1 := (m_{1,1}, ..., m_{1,N})^T$ and $\mathcal{M}_2 := (m_{2,1}, ..., m_{2,N})^T$.

The scalar potential V is discretized analogously. It is calculated at each iteration step separately by means of the relation $\Delta V = M_S \text{div}\ (\chi_\Omega \mathbf{m})$, see section ref. Since it is defined on the domain $\Omega \cup \Omega_V$, additional basis functions η_j, $j = N + 1..N_V$ are necessary such that

$$V_h(\mathbf{x}) = \sum_{j=1}^{N_V} v_j \cdot \eta_j(\mathbf{x})$$

and $\mathcal{V} := (v_1, ..v_{N_V})$ is the respective coefficient vector.

B.2 Elementwise calculation

Be $\mathcal{T}_h$ a feasible triangulation over Ω under the terms of definitions 4.1 and 4.2 and be $\mathbf{x}_j$, $j = 1...N$, the nodes of $\mathcal{T}_h$, where N denotes the total number of nodes. Since Ω is a closed polygonal domain $\Omega = \bigcup_{k=1}^{M} K_k$ holds, where K_k, $k = 1...M$, are the triangular elements of $\mathcal{T}_h$. Then

$$\int_\Omega \varepsilon^{loc}(u, \mathbf{m})\ d\mathbf{x} = \sum_{k=1}^{M} \int_{K_k} \varepsilon^{loc}(u, \mathbf{m})\ d\mathbf{x}$$

holds. Thus in this appendix the integration is only shown for one triangle K, where the nodes are w.l.o.g. (x_1, y_1), (x_2, y_2) and (x_3, y_3), and where the nonzero basis functions are η_1, η_2 and

η_3. These basis functions are locally given by

$$\begin{aligned}\eta_j(x,y) &= \frac{1}{T_z}\det\begin{pmatrix}1 & x & y\\ 1 & x_{j+1} & y_{j+1}\\ 1 & x_{j+2} & y_{j+2}\end{pmatrix}, \quad \text{where}\\ T_z &= \det\begin{pmatrix}1 & x_j & y_j\\ 1 & x_{j+1} & y_{j+1}\\ 1 & x_{j+2} & y_{j+2}\end{pmatrix} = 2\cdot\int_K 1\; d\mathbf{x}\end{aligned}$$

and the indices are modulo 3.

The functions u, $\mathbf{m}$ and V are replaced in (B.1) by their piecewise linear approximations $u_h(\mathbf{x}) = \sum_{j=1}^{3} u_j \cdot \eta_j(\mathbf{x})$, $\mathbf{m}_h(\mathbf{x}) = \sum_{j=1}^{3} \mathbf{m}_j \cdot \eta_j(\mathbf{x})$ and $V_h(\mathbf{x}) = \sum_{j=1}^{3} v_j \cdot \eta_j(\mathbf{x})$ and thus the integral over triangle K is given by

$$\begin{aligned}\int_K \varepsilon^{loc}(u_h,\mathbf{m}_h)\; d\mathbf{x} &= \int_K \frac{\varepsilon_4^2}{4}\left|\sum_{j=1}^{3} u_j\cdot\nabla\eta_j(\mathbf{x})\right|^4 + \frac{\varepsilon_2^2}{2}\left|\sum_{j=1}^{3} u_j\cdot\nabla\eta_j(\mathbf{x})\right|^2 + W\left(\sum_{j=1}^{3} u_j\cdot\eta_j(\mathbf{x})\right)\\ &+ \left[A\left|\left(\sum_{j=1}^{3}\mathbf{m}_j\cdot\nabla\eta_j(\mathbf{x})\right)\right|^2 - J_S\mathbf{H_{ext}}\cdot\left(\sum_{j=1}^{3}\mathbf{m}_j\cdot\eta_j(\mathbf{x})\right)\right.\\ &+ \left.\frac{1}{2}J_S\left(\sum_{j=1}^{3}\mathbf{v}_j\cdot\nabla\eta_j(\mathbf{x})\right)\cdot\left(\sum_{j=1}^{3}\mathbf{m}_j\cdot\eta_j(\mathbf{x})\right)\right]\cdot\left(\sum_{j=1}^{3}u_j\cdot\eta_j(\mathbf{x})\right)\; d\mathbf{x}\end{aligned}$$

B.3 Transformation

To conduct the integration, the triangle K is mapped to the standard triangle K_S with vertices $(0,0)$, $(1,0)$, $(0,1)$. The change of variables formula is stated in the following theorem:

Theorem B.1. *Let U, V be open sets in R^n and Φ: $U \to V$ an injective differentiable function with continuous partial derivatives, the Jacobian of which is nonzero for every x in U. Then for*

any real-valued, compactly supported, continuous function f, with support connected in $\Phi(U)$,

$$\int_{\Phi(U)} f(\mathbf{v})\, d\mathbf{v} = \int_{U} f(\Phi(\mathbf{u}))\, |\det(\mathrm{D}\,\Phi)(\mathbf{u})|\, d\mathbf{u}. \tag{B.3}$$

This theorem is applied on triangle K with vertices (x_1, y_1), (x_2, y_2), (x_3, y_3) and on the corresponding basis functions. The transformation function is defined as

$$\Phi(s,t) = \begin{pmatrix} x_1 \\ \\ y_1 \end{pmatrix} + \begin{pmatrix} x_2 - x_1 \\ \\ y_2 - y_1 \end{pmatrix} s + \begin{pmatrix} x_3 - x_1 \\ \\ y_3 - y_1 \end{pmatrix} t$$

Let (s,t) be the new coordinate in K_S, where $s+t \leq 1$ holds and $\mathbf{x} = (x,y)$ be the corresponding coordinate in K. Then

$$\begin{aligned} \Phi : K_S &\rightarrow K \ , \\ \Phi(s,t) &= \mathbf{x} \ , \\ |\det(\mathrm{D}\,\Phi)| &= \left| \det \begin{pmatrix} x_2 - x_1 & x_3 - x_1 \\ \\ y_2 - y_1 & y_3 - y_1 \end{pmatrix} \right| = T_z \ , \end{aligned}$$

and equation (B.3) is here

$$\int_K f(\mathbf{x})\, d\mathbf{x} = T_z \int_0^1 \int_0^{1-t} f(\Phi(s,t))\, ds\, dt$$

Bibliography

[1] Feynman R.

There's plenty room at the bottom

Talk given on december 29th 1959 at Caltech

http://www.zyvex.com/nanotech/feynman.html

[2] Children's Hospital of Philadelphia

Magnetically Guided Nanoparticles May Deliver Treatment To Organs

ScienceDaily 8 January 2008

http://www.sciencedaily.com/releases/2008/01/080107181557.htm

[3] Kyrtatos P.G., Lehtolainen P., Junemann-Ramirez M. et al.

Magnetic Tagging Increases Delivery of Circulating Progenitors in Vascular Injury

JACC Cardiovascular Interventions Vol.2, Iss.8 (2009)

[4] Cahn J.W., Hilliard J.E.

Free Energy of a Nonuniform System. I. Interfacial Free Energy

J. of Chem. Phys Vol. 28 (1958), p. 258 - 267

[5] Cahn J.W., Hilliard J.E.

Free Energy of a Nonuniform System. III. Nucleation in a Two-Component Imcompressible

Fluid

J. of Chem. Phys Vol. 31 (1959), p. 688-699

[6] Lu A.-H., Salabas E.L., Schüth F.

Magnetische Nanopartikel: Synthese, Stabilisierung, Funktionalisierung und Anwendung

Angew. Chem. 119 (2007), p. 1242-1266

[7] Hilgendorff M., Giersig M.

Assemblies of Magnetic Particles: Synthesis and production

Ch. 15 in "Nanoscale materials" by Liz-Marzan L.M., Kamat P.V.

Springer Netherlands, 2002

[8] Hilgendorff M., Tesche B., Giersig M.

Creation of 3-D Crystals from Single Cobalt Nanoparticles in External Magnetic Fields

Aust. J. Chem. 54 (2001), p. 497-501

[9] Hilgendorff M., Giersig M.

Assemblies of Magnetic Particles: Properties and Applications

Ch. 14 in "Nanoparticle Assemblies and Superstructure" by Kotov N.

Marcel Dekker Inc, 2005

[10] Hayes C.F.

Observation of Association in a Ferromagnetic Colloid

J. Colloid Interface Sci. 52 (1975), p. 239-243

[11] Satoh A., Chantrell R.W., Kamiyama S.-I., Coverdale G.N.

Two-Dimensional Monte Carlo Simulations to Capture Thick Chainlike Clusters of Ferromagnetic Particles in Colloidal Dispersions

J. Colloid Interface Sci. 178 (1996), p. 620-627

[12] Kittel Ch.

Introduction to solid state physics,

John Wiley & Sons, Inc, 8th edition, 2005

[13] Raith W.

Bergmann Schaefer, Lehrbuch der Experimentalphysik, Band 2: Elektromagnetismus

de Gruyter, 9th edition, 2006

[14] Hubert A., Schäfer R.

Magnetic Domains

Springer, 1998

[15] Brown W.F.Jr.

Micromagnetics

Interscience publishers, 1963

[16] Lu H. M., Zheng W. T., Jiang Q.

Saturation magnetization of ferromagnetic and ferrimagnetic nanocrystals at room temperature

J. Phys. D: Appl. Phys 40 (2007), p. 320-325

[17] Leslie A.

Magnetic Properties of Nanostructured Materials

Chem. Mater. 8 (1996), p. 1770-1783

[18] Strassacker G., Süsse R.

Rotation, Divergenz und Gradient

Teubner, 2003

[19] Abinandanan T.A., Haider F.

An extended Cahn-Hilliard model for interfaces with cubic anisotropy

Philosophical Magazine A Vol. 81, No. 10 (2001), p. 2457-2479

[20] Dacorogna B.

Direct Methods in the Calculus of Variations

Springer, 1989

[21] Blanchard P., Brüning E.

Direkte Methoden der Variationsrechnung

Springer, 1982

[22] Kufner A., John O., Fučík S.

Function Spaces

Noordhoff International Publishing, 1977

[23] Ciarlet P.

The Finite Element Method for Elliptic Problems

North-Holland, Amsterdam, 1978

[24] Braess D.

Finite Elemente

Springer, 2002

[25] Kružík M., Prohl A.

Recent Developments in the Modeling, Analysis, and Numerics of Ferromagnetism

SIAM Review Vol. 48, No. 3 (2006), p. 439-483

[26] Carstensen C., Prohl A.

Numerical analysis of relaxed micromagnetics by penalised finite elements

Numerische Mathematik Vol. 90 (2001), p. 65-99

[27] Praetorius D.

Analysis of the Operator Δ^{-1}div Arising in Magnetic Models

Zeitschrift für Analysis und ihre Anwendungen

Journal for Analysis and its Applications Vol. 23, No. 3 (2004), p. 589-605

[28] C. Geuzaine and J.-F. Remacle

Gmsh: a three-dimensional finite element mesh generator with built-in pre- and post-processing facilities

1997-2009

[29] Jungnickel D.

Optimierungsmethoden

Springer, 2008

[30] Ruszczyński A.

Nonlinear Optimization

Princeton University Press, 2006

[31] Coleman T.F., Zhang Y.

Optimization Toolbox^{TM} 4 User's Guide

The MathWorks, Inc., 1984-2004

http://www.mathworks.com/access/helpdesk/help/pdf_doc/optim/optim_tb.pdf

[32] Alberty J., Carstensen C., Funken S.A.

Remarks around 50 lines of Matlab: short finite element implementation

Numerical Algorithms 20 (1999), p. 117-137

[33] Lootsma F.A.

Numerical Methods for Non-linear Optimization

Academic Press, 1972

[34] Byrd R.H., Gilbert J.C., Nocedal J.

A trust region method based on interior point techniques for nonlinear programming

Math. Program., Ser. A, Vol. 89 (2000), p. 149-185

[35] Byrd R.H., Hribar M.E., Nocedal J.

An interior point algorithm for large-scale nonlinear programming

SIAM J. Optim., Vol. 9, No. 4 (1999), p. 877-900

[36] Waltz R.A., Morales J.L., Nocedal J., Orban D.

An interior point algorithm for nonlinear optimization that combines line search and trust region steps

Math. Program., Ser. A, Vol. 107 (2006), p. 391-408

[37] DeSimone A., Kohn R., Müller S., Otto F.

Recent analytical developments in micromagnetics

Max-Planck-Institut für Mathematik in den Naturwissenschaften

Leipzig, Preprint no. 80 (2004)